Eicosapentaenoic acid-mediated activation of PGAM2 regulates skeletal muscle growth and development via the PI3K/AKT pathway

Chenchen Li, Haigang Cao, Yingchun Ren, Jinrui Jia, Gongshe Yang, Jianjun Jin, Xin'e Shi

PII: S0141-8130(24)02352-3

DOI: https://doi.org/10.1016/j.ijbiomac.2024.131547

Reference: BIOMAC 131547

To appear in: *International Journal of Biological Macromolecules*

Received date: 12 January 2024

Revised date: 20 March 2024

Accepted date: 10 April 2024

Please cite this article as: C. Li, H. Cao, Y. Ren, et al., Eicosapentaenoic acid-mediated activation of PGAM2 regulates skeletal muscle growth and development via the PI3K/AKT pathway, *International Journal of Biological Macromolecules* (2024), https://doi.org/10.1016/j.ijbiomac.2024.131547

Eicosapentaenoic Acid-Mediated Activation of PGAM2 Regulates Skeletal Muscle Growth and Development via the PI3K/AKT Pathway

Chenchen Li[a,1], Haigang Cao[a,1], Yingchun Ren[a], Jinrui Jia[a], Gongshe Yang[a], Jianjun Jin[a,*], Xin'e Shi[a,*]

[a] Laboratory of Animal Fat Deposition and Muscle Development, Key Laboratory of Animal Genetics, Breeding and Reproduction of Shaanxi Province, College of Animal Science and Technology, Northwest A&F University, Yangling, 712100, Shaanxi, P.R. China.

[1] There authors contributed equally to this work.

* For correspondence: Xin'e Shi: xineshi@nwafu.edu.cn; Jianjun Jin: jinjianjun2021@nwafu.edu.cn.

Abstract

Eicosapentaenoic acid regulates glucose uptake in skeletal muscle and significantly affects whole-body energy metabolism. However, the underlying molecular mechanism remains unclear. Here we report that eicosapentaenoic acid activates phosphoglycerate mutase 2, which mediates the conversion of 2-phosphoglycerate into 3-phosphoglycerate. This enzyme plays a pivotal role in glycerol degradation, thereby facilitating the proliferation and differentiation of satellite cells in skeletal muscle. Interestingly, phosphoglycerate mutase 2 inhibits mitochondrial metabolism, promoting the formation of fast-type muscle fibers. Treatment with eicosapentaenoic acid and phosphoglycerate mutase 2 knockdown induced opposite transcriptomic changes, most of which were enriched in the PI3K-AKT signaling pathway. Phosphoglycerate mutase 2 activated the PI3K-AKT signaling pathway, which inhibited the phosphorylation of FOXO1, and, in turn, inhibited mitochondrial function and promoted the formation of fast-type muscle fibers. Our results suggest that eicosapentaenoic acid promotes skeletal muscle growth and regulates glucose metabolism by targeting phosphoglycerate mutase 2 and activating the PI3K/AKT signaling pathway.

Graphical abstract

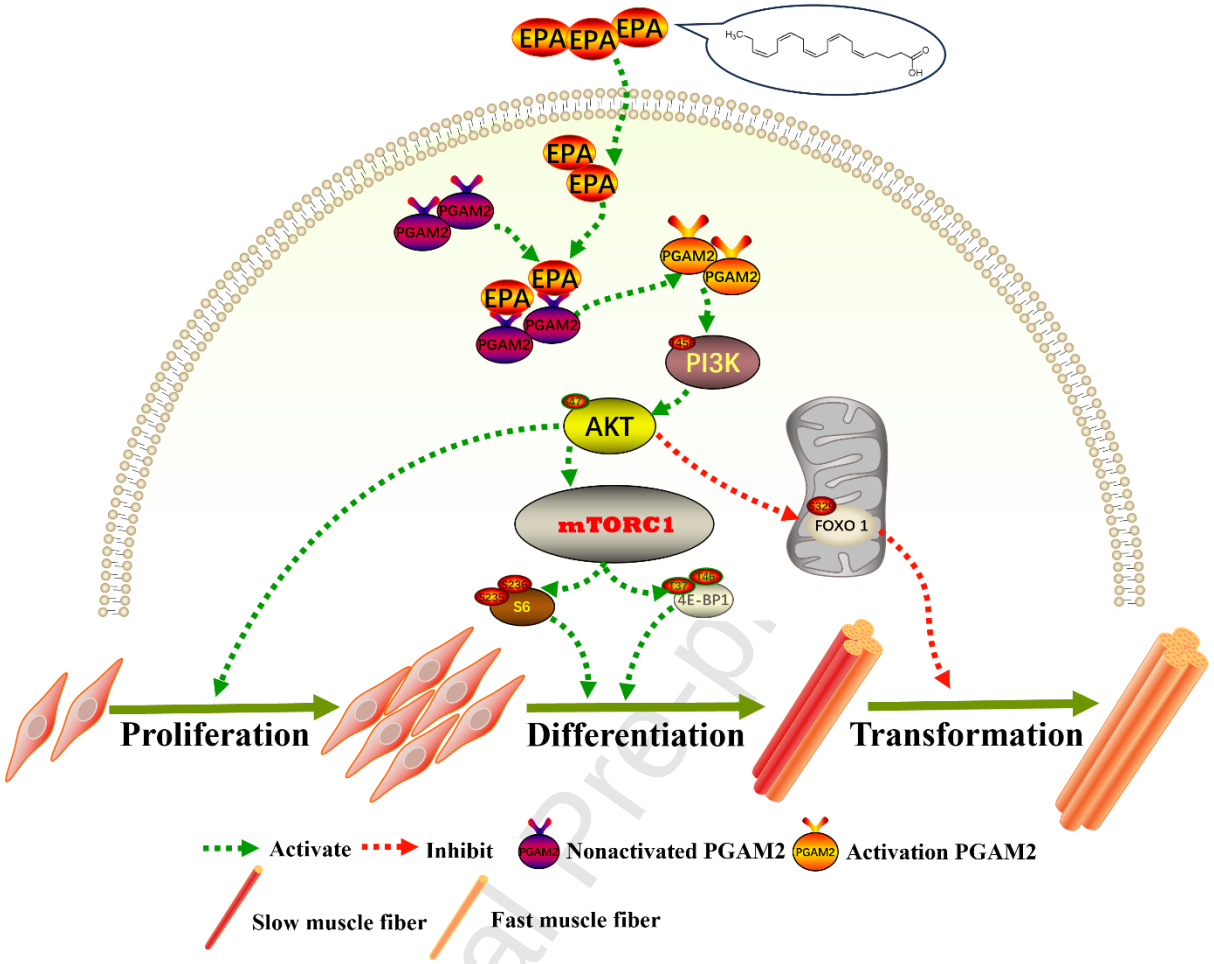

Keywords

eicosapentaenoic acid; phosphoglycerate mutase 2; myogenesis; muscle fiber type transformation; mitochondria

1. Introduction

Skeletal muscle accounts for about 40% of the body weight of mammals and is the main source of animal protein for human consumption. Skeletal muscle is essential for metabolism, homeostasis, and motion. It has high tissue activity and plasticity, but abnormal development leads to metabolic disorders, which cause several number of muscle and metabolic diseases[1]. The growth and development of skeletal muscle is a complex and sequential process that is influenced by regulatory factors, such as paired box 7 [2] and myogenic regulatory factors [3], as well as signaling pathways, such as the PI3K/AKT, MAPK, and JAK/STAT pathways [4].

The process involves the proliferation, differentiation, and fusion of skeletal muscle satellite cells (MuSCs), resulting in the formation of myofibers [5].

Myofibers are the basic functional unit of skeletal muscle, and their number remains constant after birth in mammals. Postnatal muscle growth is principally mediated by hypertrophy of muscle fibers and transformation of myofiber types. According to the expression pattern of myosin heavy chain (MyHC) and metabolic characteristics, myofibers are classified into slow oxidizing (MyHC I), fast oxidizing (MyHC IIa), intermediate (MyHC IIx), and fast glycolytic (MyHC IIb) myofibers [6]. The proportion of myofibers in skeletal muscle affects meat quality and muscle strength [7]. Different types of muscle fibers, their structure, contraction characteristics, and average cross-sectional area are different, which also directly determines the meat quality [8]. Compared with other types of muscle fibers, slow muscle fibers contain more myoglobin and mitochondria, have a smaller average cross-sectional area, and have higher oxidative metabolic enzyme activity [6, 9]. Meat containing a large number of slow muscle fibers is red, with relatively good sensory quality [10], and a strong ability to resist fatigue during exercise. In contrast, the average cross-sectional area of fast glycolytic muscle fibers is larger, which produces explosive power. To adapt to external stimuli, the proportion of muscle fibers in skeletal muscle changes. For example, peroxisome receptor proliferation-activated receptor gamma coactivator-1α (PGC-1α) promotes mitochondrial biosynthesis, aerobic metabolism, and the formation of slow-type myofibers [11].

Fish oil is rich in n-3 polyunsaturated fatty acids (PUFAs) and has a high profile in medicine and animal husbandry. Supplementing with fish oil enhances muscle mass and function in the elderly [12], and n-3 PUFAs improves mitochondrial autophagy, which regulates mitochondrial function and inhibits muscle atrophy [13]. Supplementation feed with fish oil inhibits pro-inflammatory and endoplasmic reticulum stress signaling pathways in the liver of lactating sows [14]. Eicosapentaenoic acid (EPA), the active ingredient in fish oil, improves skeletal muscle function and enhances muscle mass and strength [15]. EPA improves glucose uptake in the skeletal muscle of mice, thus affecting systemic metabolism [16]. EPA inhibits inflammation when skeletal muscle is inflamed and injured, and promotes protein synthesis and skeletal muscle regeneration [17, 18]. Although EPA is beneficial for muscle function and growth, the underlying target genes and molecular mechanisms remain unclear.

The energy metabolism of skeletal muscle affects whole-body metabolism, and glucose

metabolism is the main mode of energy metabolism. Phosphoglycerate mutase 2 (PGAM2) mediates the conversion of 2-phosphoglycerate to 3-phosphoglycerate by transferring the phosphate group from the third carbon to the second carbon of the glycine molecule and is the main enzyme in glycerol degradation [19]. *PGAM2* is autosomal recessive, and mutations cause muscle weakness, myoglobinuria, and muscle spasms [20]. Intranuclear PGAM2 is an important regulator of recovery after surgery from hepatocellular carcinoma and is associated with cirrhosis, low-grade dysplastic nodules, highly dysplastic nodules, and hepatocellular carcinoma [21]. Porcine *PGAM2* is mainly expressed in muscle tissues (skeletal and cardiac muscle) [22]. Fontanesi *et al.* analyzed the association between the candidate gene for glycolysis potential and production traits such as meat-quality parameters, daily gain, and feed conversion rate in pigs. *PGAM2* expression affected growth rate, feed conversion rate, and slaughter traits [23]. In another study, *PGAM2* expression was negatively associated with beef tenderness, making it a potential biomarker of beef quality [24]. However, the effect of PGAM2 on muscle growth and muscle fiber formation and the underlying molecular mechanism(s) are unclear and require further investigation.

Here, we report that EPA promotes the proliferation and differentiation of porcine MuSCs and fast myofiber formation. We used molecular docking analysis to identify *PGAM2 as* the EPA target gene; EPA targeted and activated *PGAM2*, thereby regulating the proliferation and differentiation of MuSCs via the PI3K/AKT pathway and promoting the transformation of myofiber types.

2. Materials and methods

2.1. Experimental animals

The longissimus dorsi (LD) and soleus (SOL) muscle tissues from four healthy male Large White pigs (180 days) were collected from a slaughterhouse (Yangling, Shaanxi, China) and stored in liquid nitrogen. In addition, 3- to 5-day-old Large White pigs were purchased and euthanized with an overdose of intravenous sodium pentobarbital (>150 mg/kg) for isolation and culture of porcine primary muscle cells. Seven-week-old male C57BL/6J mice were purchased from Chongqing Tengxin Biotechnology Co. and maintained at a room temperature of 25°C and under a 12 h/12 h light-dark cycle. The feed was purchased from Synergistic Pharmaceuticals & Biologicals Co. Ltd (Jiangsu, China), and met the standard for experimental mouse growth and reproduction feed. The mice were housed 4–5 mice per cage and offered water *ad libitum*. After 1 week of acclimatization (8 weeks of age), the adeno-associated virus

was injected into the leg muscles, and EPA gavage experiments were performed (0.5 mg/mouse, once every 2 days). Five groups were randomly assigned with free choice of diet, including the blank control group (CON), the AAV-NC adeno-associated virus injection and the gavage DMSO group (ND), the AAV-si-PGAM2 adeno-associated virus injection and gavage DMSO group (NS), the AAV-NC adeno-associated virus injection and gavage EPA group (NE), and the AAV-si-PGAM2 adeno-associated virus injection and gavage EPA group. Body weights were measured weekly. Exercise training was performed during 1 week of acclimatization (week 16), and exercise-related indices were measured on week 17. By week 18, the mice weights had stabilized and the animals were euthanized (deep anesthesia with isoflurane (5%) and exsanguination during anesthesia) to collect the samples. All animal studies were approved by the Institutional Animal Care and Use Committee of the Northwest A & F University (XN2024-0304). All applicable institutional and/or national guidelines for the care and use of animals were followed, and we complied with all relevant ethical regulations for animal experimentation.

2.2. Drugs and chemicals

EPA (Shanghai Yuanye, S27566) is a free fatty acid with the molecular formula ($C_{20}H_{30}O_2$). Canonical SMILES (CCC=CCC=CCC=CCC=CCC=CCC=CCC(=O)O), were dissolved in DMSO, and diluted with DMEM or PBS. The PI3K/AKT signaling pathway inhibitor was purchased from APEXBIO (A3432, GDC-0941), dissolved in DMSO, and diluted in DMEM.

2.3. Cell isolation and culture

We used healthy male white pigs 3–5 days after birth to obtain the muscle cells after euthanasia. First, we separated the leg and LD muscles, which were cut into small fragments using scissors. The tissue fragments were digested with 0.2% type II collagenase for 2 h and the resulting cell suspension was passed through a sieve. The isolated cells were cultured in RPMI medium 1640 basic (Gibco, Grand Island, NY, USA) with 20% fetal bovine serum (Gibco) and 1% penicillin/streptomycin. C2C12 cells (Shanghai Branch Cell Bank of the Chinese Academy of Sciences) were cultured in DMEM (Cytiva, Marlborough, MA, USA) with 10% fetal bovine serum and 1% penicillin/streptomycin. MuSCs and C2C12 cells were to 90% confluence to induce the formation of myotubes. The culture medium was exchanged for DME/F-12 (Cytiva) containing 2% horse serum for 3 days.

2.4. Quantitative polymerase chain reaction

Total RNA was isolated from cell and muscle samples using the AG RNAex Pro RNA Reagent

(Accurate Biotechnology, Beijing, China) and reverse transcribed into cDNA according to the manufacturer's instructions (Novozymes Biotechnology, Shanghai, China). The expression levels of the genes of interest were normalized to the *18S* reference gene, and relative expression was calculated using the ΔΔCt method. The primer sequences used for q-RT-PCR were as follows:

Oligo	Sequences (5'—3')	Tm(℃)
PGMA2	F:TGCCCTTCTGGAACGATGAG R:TCCAGATGCTTGACGATGCC	60
18sRNA	F:CCCACGGAATCGAGAAAGAG R:TTGACGGAAGGGCACCA	60
Cyclin B	F:AATCCCTTCTTGTGGTTA R:CTTAGATGTGGCATACTTG	60
Cyclin D	F:TACACCGACAACTCCATCCG R:GAGGGCGGGTTGGAAATGAA	60
Cyclin E	F:AGAAGGAAAGGGATGCGAAGG R:CCAAGGCTGATTGCCACACT	60
PCNA	F:GCAGAGCATGGACTCGTCTC R:TTGGACATGCTGGTGAGGTT	60
CDK4	F:TTGTCCGGCTGATGGATGTC R:GCTCAAACACCAGGGTCACT	60
p21	F:TGTCAGAGTCGACCAGGGAT R:CACATGGTCCTCCTGAGACG	60
p27	F:GTCCCTTTCAGTGAGAACCGATAC R:TTGCTGCCACATAACGGAATCAT	60
MYHC	F:TTGAAAAGACGAAGCAGCGAC R:AGAGAGCGGGACTCCTTCTG	60
MYOD	F:GGCTGCCCAAGGTGGAAATC R:TGCGTCTGAGTCACCGCTGTAG	60
MYOG	F:ATGAGACATCCCCCTACTTCTACCA R:GTCCCCAGCCCCTTATCTTCC	60
MYF5	F:AGCGTGCAAGAGGAAATCCA R:CAGCCTCTGGTTGGGGTTAG	60
MYHC Ⅰ	F:AAGGGCTTGAACGAGGAGTAGA R:TTATTCTGCTTCCTCCAAAGGG	60
	F:GCTGAGCGAGCTGAAATCC	60

MYHC Ⅱa	R:ACTGAGACACCAGAGCTTCT	
MYHC Ⅱx	F:AGAAGATCAACTGAGTGAACT R:AGAGCTGAGAAACTAACGTG	60
MYHC Ⅱb	F:ATGAAGAGGAACCACATTA R:TTATTGCCTCAGTAGCTTG	60
SDHB	F:ACAGCTCCCCGAATCAAGAA R:CTCCGTTGATGTTCATGGCG	60
NDUFB8	F:GTGTAAGCACCTCTCCGGTT R:TTCTTTGGTAGGATCGCCGC	60
UQCRC2	F:CAACCCTGAGCAGCAAATACG R:GTAACCAGAGCCACACCAGT	60
NDUFA1	F:ACCTGGTCCGTTGTCTTTCC R:TCTCGAACGCTTGAACTCCC	60
COX5A	F:CACCCGGCTTTGCCTTAGC R:GCGAATTGACTGGATAGCGG	60
CD36	F:TGTCCCTGCAACTCACAGAC R:TGTCTGCTGATGCTGTACTATGG	60
PGC-1α	F:GTACCTCCGCCATCGAAGAA R:CGAGCGCGGACGTCTTG	60

2.5. Western blotting

Cell and muscle samples were lysed in RIPA buffer (Yessen, Shanghai, China) containing a mixture of protease and phosphatase inhibitors. After centrifugation (12,000 rpm, 10 min, 4°C), the proteins were separated by 10% polyacrylamide gel electrophoresis and transferred to polyvinylidene difluoride membranes (Millipore, IPVH00010: Billerica, MA, USA). The membranes were incubated with the primary antibody overnight at 4°C followed by the secondary antibody for 1 h at room temperature and visualized using the Image Lab system. Protein band densities were quantified using ImageJ software. We used antibodies against Ki67 (Santa-Cruz Biotechnology, sc-23900; Santa Cruz, CA,USA), cyclin B (Proteintech, 55004–1-AP; Rocky Hill, NJ, USA), CDK4 (Abways, CY5827; Shanghai, China), P21 (Abways, CY5088), β-tubulin (Abways, CY5088), MyHC (R&D Systems, MAB4470; Minneapolis MN, USA), MyoG (Novus Biologicals, NB100–56510, Wilmington, DE, USA), MyoD (Novus Biologicals, NBP1–54153), MYF5 (Abcam, ab125301; Cambridge, MA, USA), MYHC-fast (Merck, M4276; Parsippany, NJ, USA), MYHC-slow (Merck, M8421), ATP5A (PTMBIO, PTM-5163; Hangzhou, China), UQCRC2 (PTMBIO, PTM-5008), MTCO1 (PTMBIO, PTM-

5109), SDHB (PTMBIO, PTM-5164), NDUFB8 (PTMBIO, PTM-5899), PGAM2 (Bioss, bs-23502R, PTMBIO, PTM-6768), PGK1 (Proteintech, 17811–1-AP), MYH7 (DSHB, BA-D5), MYH2 (DSHB, SC-71), MYH1 (Proteintech, 25182–1-AP), MYH4(DSHB, 10F5), p-PI3K (Affinity Biosciences, AF3242; Shanghai, China), PI3K (PTMBIO, PTM-6358), p-AKT (PTMBIO, PTM-6649), AKT (PTMBIO, PTM-6470), p-S6 (PTMBIO, PTM-5321), S6 (PTMBIO, PTM-5862), p-4E-BP1 (PTMBIO, PTM-6515), 4E-BP1 (PTMBIO, PTM-5620), p-FOXO1 (Affinity Biosciences, AF3416), and FOXO1 (Proteintech, 18592–1-AP). The HRP-conjugated goat anti-mouse and anti-rabbit IgG secondary antibodies were obtained from BOSTER (Beijing, China).

2.6. Flow cytometry

Cells were digested with a pancreatic enzyme in 1.5 mL centrifuge tubes, washed twice with pre-cooled PBS, centrifuged (1,500 rpm, 5 min, 4°C), with 1 mL of pre-cooled 70% ethanol, and fixed for 12 h. The cells were centrifuged (1,500 rpm, 5 min, 4°C), and the supernatant was discarded. The cells were rinsed with pre-cooled PBS and stained with a cell cycle kit (Beyotime, Shanghai, China). The cells were transferred to a water bath at 37℃ for 30 min and subjected to flow cytometry (BD Biosciences, Santa Clara, CA, USA) [25].

2.7. 5-Ethynyl-2'-deoxyuridine staining

The C10310 EdU Apollo *In vitro* Imaging Kit (RiboBio, Shanghai, China) was used for 5-ethynyl-2'-deoxyuridine (Edu) staining. Edu (solution A) was diluted 1,000:1 with cell culture medium, and the cells were cultured for 2 h and then washed twice in PBS. Next, the cells were fixed in 4% paraformaldehyde for 30 min, decolorized with 2 mg/mL glycine for 5 min, decolorized in PBS with 0.5% Triton-100 for 10 min, and washed with PBS. Apollo staining solution (1×) was added, and the cells were incubated for 30 min and then washed with PBS. Hoechst stain was added, and the cells were washed three times with PBS and photographed using Cellens software (Olympus Corp., Tokyo, Japan) [25].

2.8. Cell counting kit-8 assay

The cells were cultured to 80% density in 96-well cell culture plates. A 10 μL aliquot of TransDetect Cell Counting Kit reagent (TransGen, Beijing, China) was added to each well. The plates were incubated at 37℃ for 2 h, and the absorbance was measured.

2.9. Immunofluorescence staining

MuSCs and C2C12 cells were fixed in 4% paraformaldehyde, permeabilized with 0.5% Triton X-100, and incubated with anti-MyHC and anti-PGAM2 antibodies overnight at 4°C. After the

incubation with a secondary antibody, the nuclei were stained with 2 μg/mL 12,10-diamidino-4-phenylindole (DAPI) and photographed using Cellens software. We used an antibody against MyHC (R&D Systems, MAB4470) and a FITC-conjugated goat anti-mouse IgG (EK013) [25].

2.10. Tissue section staining

For H&E staining, fresh tibialis anterior (TA) and Gastrocnemius (GAS) muscle tissues were fixed in 4% paraformaldehyde for more than 48 h, followed by dehydration and embedding. Paraffin sections of muscle of 2 to 4 μm thickness were produced for HE staining, and digital images were obtained using a Panoramic DESK scanner (P-MIDI, P250, 3D HISTECH, Budapest, Hungary).

Fresh SOL and GAS muscles were transferred to OCT embedding agent for tissue immunofluorescence staining, embedded in isopentane, and frozen in liquid nitrogen. Then, 20 μm muscle samples were cut with a frozen microtome (Sakura, Tokyo, Japan). The sections were incubated with anti-MYHC7, anti-MYHC2, and anti-MYHC4 primary antibodies overnight, and subsequently with a fluorophore-conjugated secondary antibody for 1 h; they were photographed using Cellens software. We used antibodies against MYH7 (DSHB, BA-D5, Des Moines, IA, USA), MYH2 (DSHB, SC-71), and MYH4 (DSHB, 10F5), together with AlexaFluor 594 goat anti-mouse IgM (Immunoway, RS3609, Plano, TX, USA), goat anti-mouse IgG1 cross-adsorbed (Thermo Fisher, A-21121, Waltham, MA, USA), and goat anti-mouse IgG2b cross-adsorbed (Thermo Fisher, A-21140) secondary antibodies [26].

2.11. Transmission electron microscopy

Fresh cell samples were transferred to 1.5 mL centrifuge tubes and fixed in 3% glutaraldehyde. The samples were post-fixed in 1% osmium tetraoxide in 0.1 M sodium cacodylate buffer. After overnight incubation in 0.5% uranyl acetate, the samples were dehydrated in ethanol and propylene oxide and polymerized in Spurr's resin at 70°C. The sample were prepared was performed by LiLai (Chengdu, China) [27].

2.12. Mitochondrial copy number

Total DNA was extracted with a tissue DNA kit (Mei5bio, Beijing, China) following the manufacturer's instructions. The amount of mitochondrial DNA was determined by quantifying *cytochrome c oxidase subunit I* (*COX1*). *GCG* was used as the internal control.

COX1 Forward: 5 ′-TCACAGCCGTACTACTTCTACTATCCC-3′

COX1 Reverse: 5′-GTGTTCAGGTTGCGGTCTGTCAG-3′

GCG Forward: 5′-ACTTTGTGGCTGGATTGTTTGTAATGC-3′

GCG Reverse: 5′-CTGGGAATGATCTGGATTTCTCCTCTG-3′

2.13. Mito Tracker

Cells were allowed to adhere to and proliferate on the walls of a culture dish to a predetermined density, and the culture medium was removed. Mito Tracker Red CMXRos (HB210924; Yessen Biotechnology, Shanghai, China) staining solution (200 nM) was added for 30 min and then replaced with fresh medium, and the cells were observed under a confocal laser scanning microscope (Andor,London, UK) [28].

2.14. RNA-seq

RNA-seq was performed by Tsingke Biotechnology Co. (Beijing, China). The raw image data files produced by high-throughput sequencing were transformed into raw sequencing sequence data (RawData) by CASAVA/Basecall_T7_GPU_1.2.0.26_Centos Base Calling analysis, and the reference genome and gene model annotation files were downloaded from the genome website and used for *de novo* gene prediction in StringTie (2.1.2). Novel genes were sequenced against the NR, Swiss-Prot, GO, COG, KOG, Pfam, and KEGG databases using BLAST (2.2.31) software. A quantitative gene expression analysis was performed using StringTie software. Differential expression analysis was performed between sample sets with biological duplicates using DEseq2 (1.26.0) software to obtain a set of differentially expressed genes (DEGs) between the two biological conditions. A differential gene set enrichment analysis (GSEA) was conducted using the Cluster Profile (3.14.3) package.

2.15. Molecular docking

Molecular docking was performed using AutoDock Vina 1.1.2 software. The receptor protein was treated with PyMol 2.5.2, before docking, including the removal of water molecules, salt ions, and small molecules. The docking box was set up to wrap the entire protein structure. In addition, ADFRsuite 1.03 was used to convert all processed small molecules and receptor proteins into the PDBQT format necessary for AutoDock Vina 1.1.2 docking. The exhaustiveness of the global search was set to 32 for docking; the other parameters were at their default settings. The output docking conformation with the highest score was considered the binding conformation, and the docking results were visualized and analyzed using PyMol 2.5.2. [29]

2.16. Metabolite and enzyme activity assays

Fresh cell samples were washed three times with PBS at 4℃ and collected in 200 μL PBS by scraping. Next, the cells were subjected to five freeze-thaw cycles in liquid nitrogen, and

centrifuged (12,000 rpm, 10 min, 4°C) to collect the supernatant. Commercial kits (HS443X-Pg, HS442X-Pg, E-120893, E-180112, and E-180110; ShangHai HengYuan Biological Technology Co., Ltd.,Shanghai, China) were used for the metabolite and enzyme activity assays according to the manufacturer's instructions.

2.17. Mouse motor training

Mice were first acclimated to a specialized treadmill (model ZH-PT, Zhenghua, Anhui, China) for 2–3 days to familiarize the mice with the apparatus and prepare them for formal training. The formal training protocol involved modulating the treadmill at an angle of 5°, the optimum for endurance training. The endurance training parameters were electric shock intensity of 0.2 mA (20 electric shocks within 30 s indicated exhaustion), acceleration rate of 1 v/s, and initial velocity of 15 m/s, with a progressive increase of 2 m/s every 5 min. Running time and the corresponding distance covered were recorded during each training session [30].

2.18. Hanging upside-down experiment

The mice were placed in the middle of a barbed wire, turned over the barbed wire, and hung upside down for measurement. The barbed wire was not less than 30 cm from the ground. The time until the mouse fell off the wire was considered the exhaustion hanging time. A bedding was placed under the barbed wire to prevent the mice from falling and injuring themselves. The maximum suspension time was 20 minu [31].

2.19. Extremity grip strength

Mice were placed on a wire mesh, and a force meter was fixed to the tail. The mice were pulled to the rear until they moved, and maximum grip strength was recorded.

2.20. Plasmids and RNA interference

si-PGAM2, si-PGK1, and the overexpressed plasmid pcDNA3.1-PGAM2 were synthesized by BTsingke Biotechnology Co., Ltd. Their sequences were

si-PGAM2: 5′ -CCUUCUGCUGUAGAACGAUGAGAUTT-3′

si-PGK1: 5′-CAGUUGCUGUAGAACUCAATT-3′

2.21. Construction and transfection of adeno-associated virus

The AAV serotype 9 vector encoding a control interference sequence (si-NC) and a short hairpin targeting PGAM2 (si-PGAM2; 5′-GCUUAUGGAACCAAGAGAATT-3′) expressing EGFP (driven by the CMV promoter) under control of the U6 promoter was obtained from Hanbio Tech (Shanghai, China). AAV2/9-expressing si-PGAM2 (40 μL) was injected intramuscularly into the TA and GAS muscles of 8-week-old mice at a titer of 1×10^{12}.

2.22. Cellular thermal shift assay（CETSA）

Skeletal muscle satellite cells were treated with EPA for 24 h. RIPA buffer containing a mixture of protease and phosphatase inhibitors (Yeson, Shanghai, China) was added, and the supernatant lysate was centrifuged, heated at a gradient or constant temperature, and then centrifuged to remove heat- and denaturation-precipitated proteins. The proteins were subjected to protein blotting for assay and quantitation, and the CETSA cleavage curve was plotted [32].

2.23. Biostatistical analysis of the data

Statistical analysis was performed using GraphPad Prism 8.02 software (Graphpad Software Inc. La Jolla, CA, US). Data are presented as mean ± SEM with the n of each group shown as an individual points or noted in the respective legends. Two group comparisons were evaluated using the two-tailed unpaired Student's t-test. Groups with multiple variables were evaluated by a two-way analysis of variance (ANOVA). The ANOVA post-hoc analysis was performed using Fisher's least significant difference test. A P-value < 0.05 was considered significantly different and $P < 0.01$ was extremely significantly different.

3. Results

3.1. EPA promotes porcine MuSC myogenesis and fast myofiber formation but suppresses mitochondrial biogenesis

To evaluate the effect of EPA on the survival of MuSCs, we treated MuSCs with the indicated concentrations of EPA. The CCK-8 assay showed that 100 μM EPA for 24 h did not have a toxic effect on MuSCs (Fig. 1A). EPA (100 μM) significantly increased the expression levels of Ki67, cyclin B, and CDK4 and decreased that of p21 (Fig. 1B). EPA significantly increased the number of EdU-positive cells (Fig. 1C). Flow cytometry indicated that EPA increased the number of cells entering S phase (Fig. 1D). Therefore, EPA promotes the proliferation of porcine MuSCs.

Next, we explored the role of EPA in myogenic differentiation. Immunofluorescence staining for MyHC indicated that EPA significantly promoted the terminal differentiation of MuSCs (Fig. 1E). In addition, EPA significantly increased the protein levels of the myogenic markers MyHC, MyoG, and Myf5 (Fig. 1F). Furthermore, EPA significantly increased the MyHC-fast protein level and decreased that of MyHC-slow (Fig. 1G). Myofiber transformation is accompanied by changes in mitochondrial function, particularly mitochondrial oxidative respiration, biogenesis, and the membrane potential [33]. EPA decreased the protein levels of

several components of the mitochondrial complexes, including ATP synthase subunit alpha (ATP5A), cytochrome b-c1 complex subunit 2 (UQCRC2), cytochrome c oxidase subunit 1 (MTCO1), succinate dehydrogenase iron-sulfur subunit (SDHB), and NADH dehydrogenase (ubiquinone) 1 beta subcomplex subunit 8 (NDUFB8) (Fig. 1H). Transmission electron microscopy showed that EPA significantly reduced the number of mitochondria (Fig. 1I), but had no significant effect on mitochondrial size, morphology, or the inner ridge structure. Mito-Tracker red mitochondrial staining indicated significantly reduced mitochondrial membrane potential in EPA-treated MuSCs compared to the control (Fig. 1J). Similarly, EPA significantly decreased mitochondrial copy number (Fig. 1K). Therefore, EPA promotes MuSC proliferation and myogenic differentiation and converts slow muscle fibers to fast muscle fibers by regulating mitochondrial biogenesis.

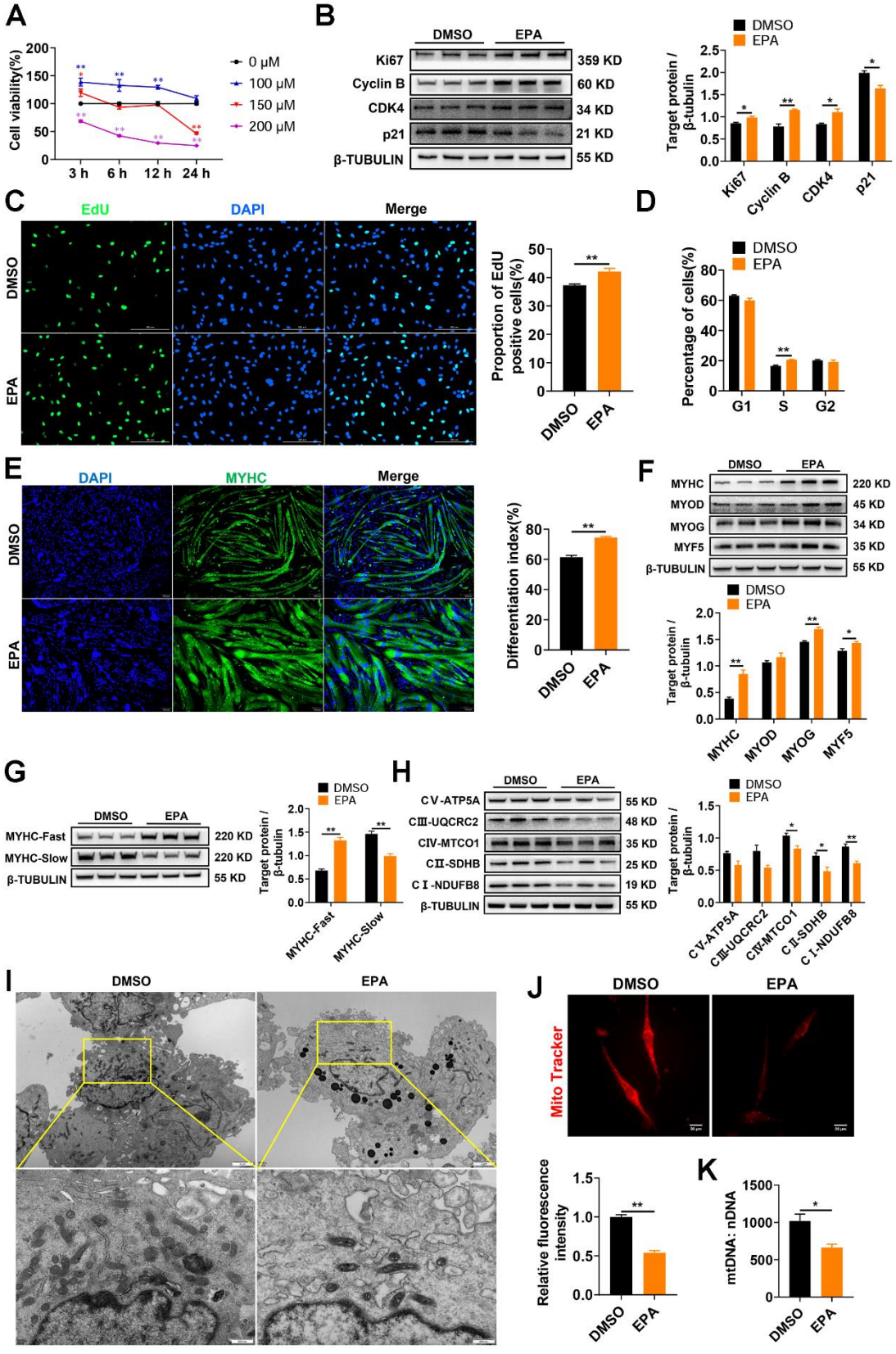

Fig. 1. EPA promotes the proliferation and differentiation of porcine MuSCs, induces glycolytic myofiber formation, and inhibits mitochondrial biogenesis. A. Effect of EPA on the viability of porcine MuSCs (*n* = 9). B. The protein levels of Ki67, cyclin B, CDK4, and p21 in MuSCs treated with 100 μM EPA were measured via western blotting (*n* = 3). C. 5-Ethynyl-2'- deoxyuridine (EdU) staining results showing the effect of EPA on the proliferation of MuSCs (*n* = 5). D. Flow cytometry results showing the effect of EPA on cell cycle progression in MuSCs (*n* = 3). E. Immunofluorescence staining results show the effect of EPA on the differentiation of MuSCs based on the differentiation index (*n* = 3). F. Protein levels of MyHC, MyoD, MyoG, and Myf5 after EPA

treatment as determined by western blotting (n = 3). G. Protein levels of MyHC-fast and MyHC-slow after EPA treatment as analyzed by western blotting (n = 3). H. Protein levels of ATP5A, UQCRC2, MTCO1, SDHB, and NDUFB8 after EPA treatment as measured by western blotting (n = 3). I. Mitochondrial morphology, size, and number of cells treated with EPA as evaluated by transmission electron microscopy. J. Mito-Tracker results showing mitochondrial membrane potential after the EPA treatment (n = 3). K. Mitochondrial copy number in MuSCs after the EPA treatment (n = 3). Results are mean ± SEM. Differences between means were detected via independent samples t-tests (*P < 0.05; **P < 0.01).

3.2. EPA functions by activating PGAM2

EPA influences glucose uptake in skeletal muscle [16], improves glucose metabolism, and affects whole-body energy metabolism [34], so we speculated that it does this by affecting the activity of a protease in the glycolytic pathway. We obtained the protein crystalline structures of the key enzymes in the glycolytic pathway from the Uniport database and the 3D structures of EPA from the PubChem database. We performed energy minimization under the MMFF94 force field. The molecular docking work was performed using AutoDock Vina 1.1.2 software, and the receptor proteins were processed using PyMol 2.5.2 before the docking started, including removing water molecules, salt ions, and small molecules. EPA had the strongest binding affinity to lactate dehydrogenase (LDHA), pyruvate kinase (PKM), and phosphoglycerate mutase 2 (PGAM2), with values of -7.1, -6.9, and -6.5 kcal/mol, respectively (Fig. 2A). No significant changes in the activities of LDHA or PKM2 were observed in the EPA-treated group (Fig. 2B-C), but the activity and total protein levels of PGAM2 increased significantly (Fig. 2D-E). EPA bound inside the helix channel of the protein, which interacts with PGAM2 at ARG-86; in addition, hydrophobic interactions between EPA and ASP-157, GLU-148, GLU-153, and ARG-161 of PGAM2 were observed (Fig. 2F).

Next, we knocked down the *PGAM2* upstream gene *phosphoglycerate kinase 1* (*PGK1*), which decreased the protein levels of PGK1 and PGAM2. Adding EPA significantly recovered PGAM2 but not PGK1 (Fig. 2G); it also did not affect the level of the upstream metabolite of PGAM2, 3-phosphoglycerate (3-PG), but significantly increased that of its downstream metabolite 2-phosphoglycerate (2-PG) (Fig. 2H–I). Finally, we used CETSA to determine that EPA had a stronger binding capacity to PGAM2 (Fig. 2J). Therefore, EPA enhances glucose metabolism by interacting with and activating PGAM2.

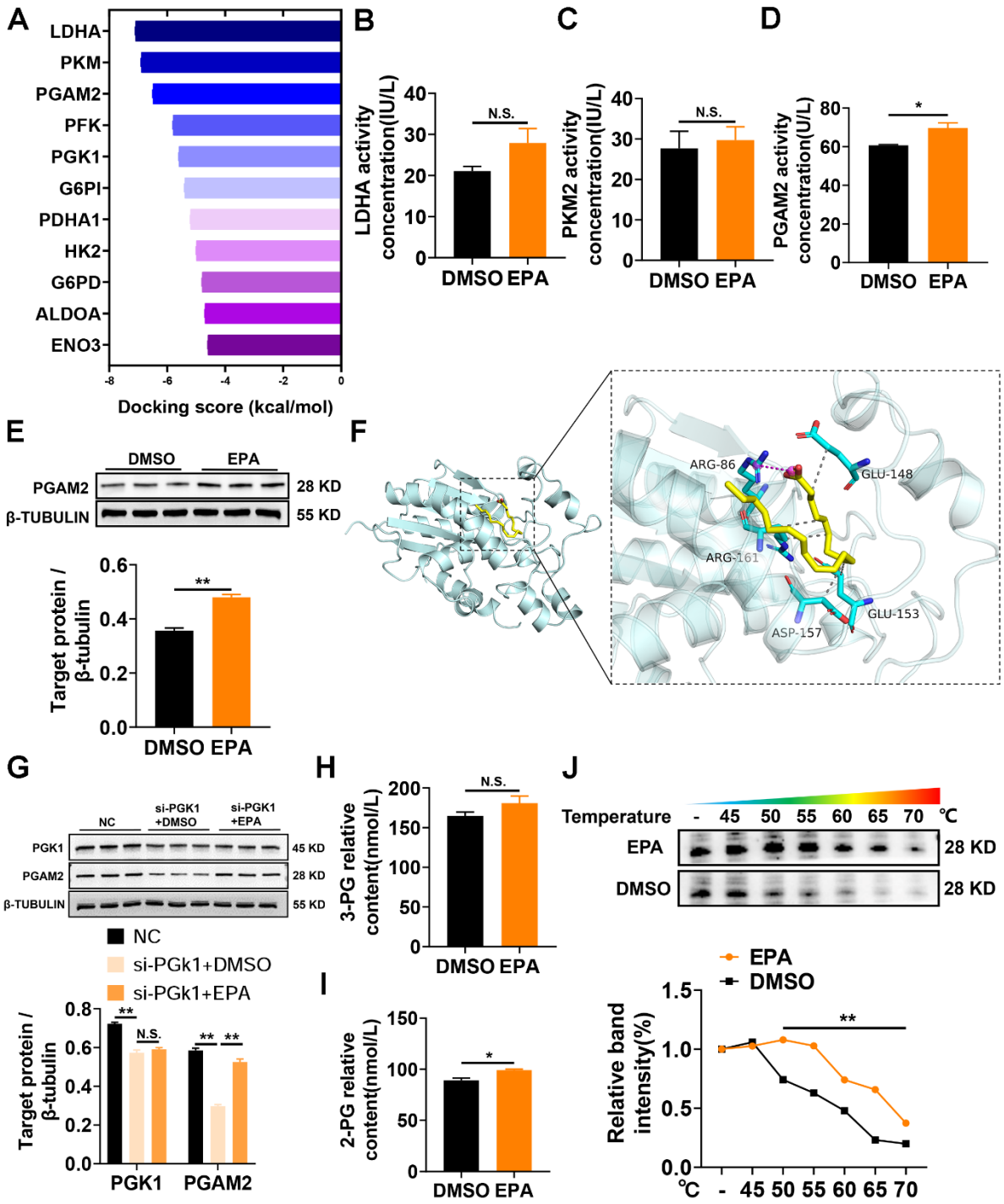

Fig. 2. EPA binds and activates PGAM2. A. Predicted binding affinity of EPA to proteases related to the glycolytic pathway. B-D. ELISA for the effect of EPA on lactate dehydrogenase (LDHA) (B), pyruvate kinase (PKM) (C), and phosphoglycerate mutase 2 (PGAM2) (D) activities (n = 3). E. The PGAM2 protein level after EPA treatment as measured by western blotting (n = 3). F. Molecular docking of EPA to PGAM2. G. Effect of adding EPA addition on the protein level of PGAM2 after knockdown of PGK1 as analyzed by western blotting (n = 3). H-I. Effect of adding EPA on the upstream and downstream metabolites of PGAM2 (n = 3). J. CETSA to determine the binding ability of EPA and PGMA2, as well as the relative band intensity curve (n = 1). Results are mean ± SEM. Differences between means were detected via independent samples t-tests (N.S. $P \geq 0.05$; *$P < 0.05$; **$P < 0.01$).

3.3. PGAM2 promotes the proliferation and differentiation of porcine MuSCs

We analyzed PGAM2 expression in the skeletal muscle of 5-month-old pigs. As results, *PGAM2* was highly expressed in skeletal muscle, particularly in the LD (fast myofibers) (Fig. 3A). Its expression fluctuated in the SOL but increased significantly in LD with age (Fig. 3B). *PGAM2* was upregulated in differentiated myotubes compared to myoblasts, suggesting that this gene plays an important role in skeletal muscle growth and the transformation of muscle fiber types (Fig. 3C).

To verify the role of *PGAM2* in myogenesis, we interfered with PGAM2 by transfecting a *PGAM2*-specific siRNA oligo (si-PGAM2). qRT-PCR showed that knockdown of PGAM2 significantly decreased the expression of the cell cycle-related genes *cyclin B*, *cyclin D*, *cyclin E*, *PCNA*, and *CDK4*, but significantly increased that of the cell cycle protein-dependent kinase inhibitor *p21* (Fig. 3D). In addition, PGAM2 knockdown significantly decreased the protein levels of the proliferation markers Ki67 and cyclin B and increased that of p21 (Fig. 3E). EdU staining and flow cytometry showed that the numbers of EdU^+ cells and S-phase cells decreased significantly after PGAM2 knockdown, indicating a significant decrease in cell proliferation (Fig. 3F-G). Next, the *PGAM2* overexpressing vectors (pcDNA3.1-PGAM2) were transfected into porcine MuSCs. qRT-PCR showed that overexpressing PGAM2 significantly increased elevated the expression of the cell cycle-related gene *cyclin B* but significantly decreased that of the cell cycle protein-dependent kinase inhibitor *p27* (Fig. 3H). The protein level of cyclin B increased significantly (Fig. 3I). In addition, the numbers of EdU^+ cells and S-phase cells increased significantly (Fig. 3J-K). These results suggest that *PGAM2* promotes the proliferation of porcine MuSCs.

To further investigate the role of PGAM2 in MuSC differentiation, we performed further *PGAM2* knockdown and overexpression assays. Knockdown of PGAM2 significantly reduced the expression levels of the myogenic marker genes *MyoD*, *MyoG*, and *Myf5* (Fig. 4A) and significantly reduced the protein levels of the myogenic markers MyHC, MyoD, MyoG, and Myf5 (Fig. 4B). Immunofluorescence staining revealed that PGAM2 knockdown significantly inhibited the differentiation of porcine MuSCs (Fig. 4C). In contrast, overexpressing PGAM2 significantly increased the expression level of the myogenic marker *MyoD* and significantly increased the protein levels of the myogenic markers MyoD, MyoG, and Myf5 (Fig. 4D-E). Immunofluorescence staining revealed that overexpressing PGAM2 significantly promoted the differentiation of porcine MuSCs (Fig. 4F). In conclusion, *PGAM2* is expressed at a high level in porcine skeletal muscle and promotes the proliferation and differentiation of porcine MuSCs.

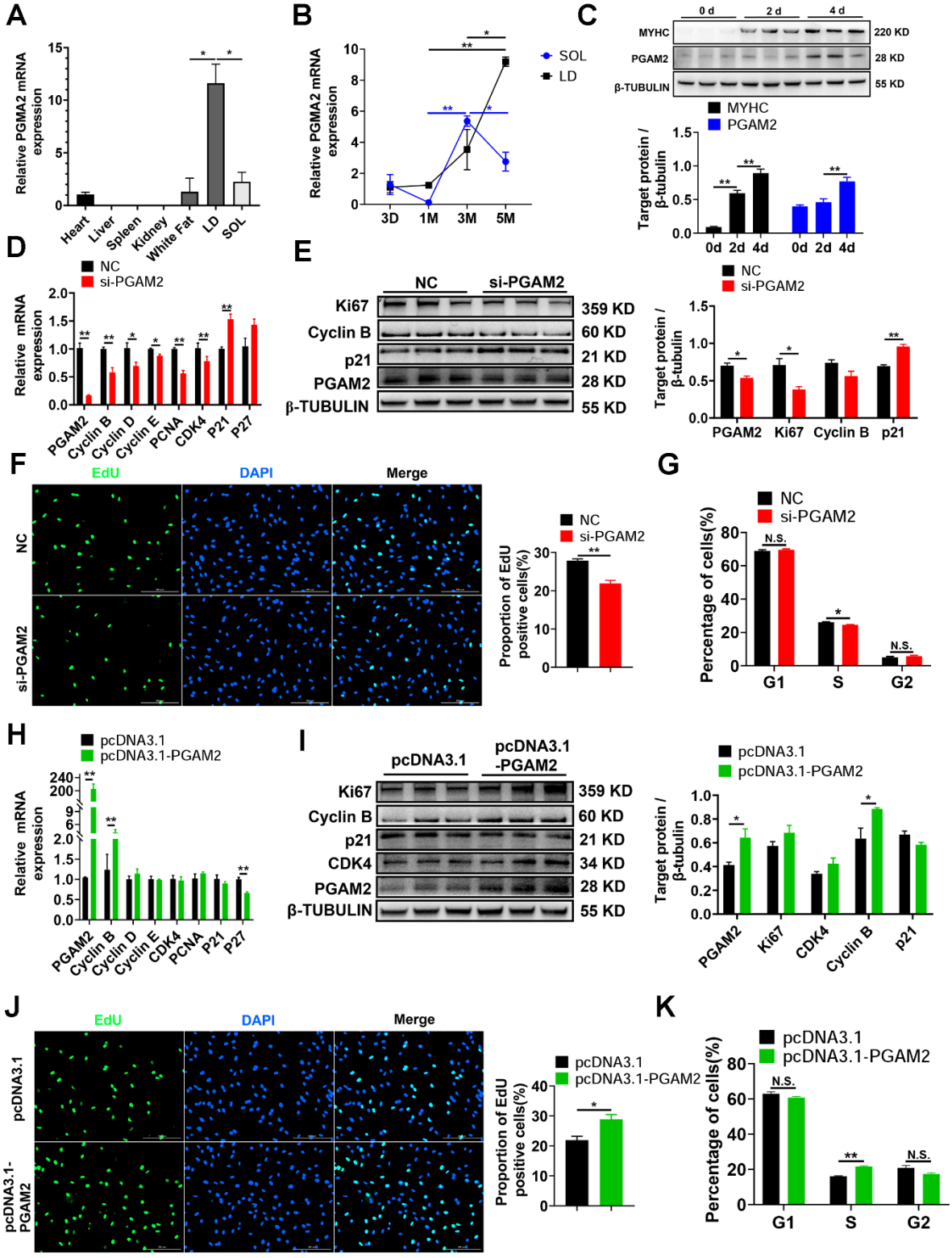

Fig. 3. PGAM2 promotes the proliferation of porcine MuSCs. A. The mRNA expression levels of *PGAM2* in pig tissues were measured by qRT-PCR (n = 3). B. The mRNA expression levels in pigs of the indicated ages as determined by qRT-PCR (n = 3; D, day; M, month). C. Protein levels of PGAM2 in porcine MuSCs at the indicated stages of differentiation as measured by western blotting (n = 3). D. The mRNA expression levels of genes associated with the cell cycle after knockdown of *PGAM2* as analyzed by qRT-PCR (n = 6). E. Protein levels of Ki67, cyclin B, and p21 after knockdown as determined by western blotting (n = 3). F. 5-Ethynyl-2'-deoxyuridine (EdU) staining after knockdown of PGAM2 in MuSC cells (n = 3). G. Flow cytometry results reflecting cell cycle progression in MuSCs after knockdown of PGAM2 (n = 3). H. The mRNA expression levels of genes associated with the cell cycle after overexpression of *PGAM2* as measured by qRT-PCR (n = 6). I. Protein

levels of Ki67, cyclin B, CDK4, and p21 after overexpression of PGAM2 as analyzed by western blotting (n = 3). J. EdU staining after overexpression of PGAM2 in MuSC cells (n = 3). K. Flow cytometry results reflecting cell cycle progression in MuSCs (n = 3). Results are mean ± SEM. Differences between means were detected by the independent samples t-tests (N.S. $P \geqslant 0.05$; *$P < 0.05$; **$P < 0.01$).

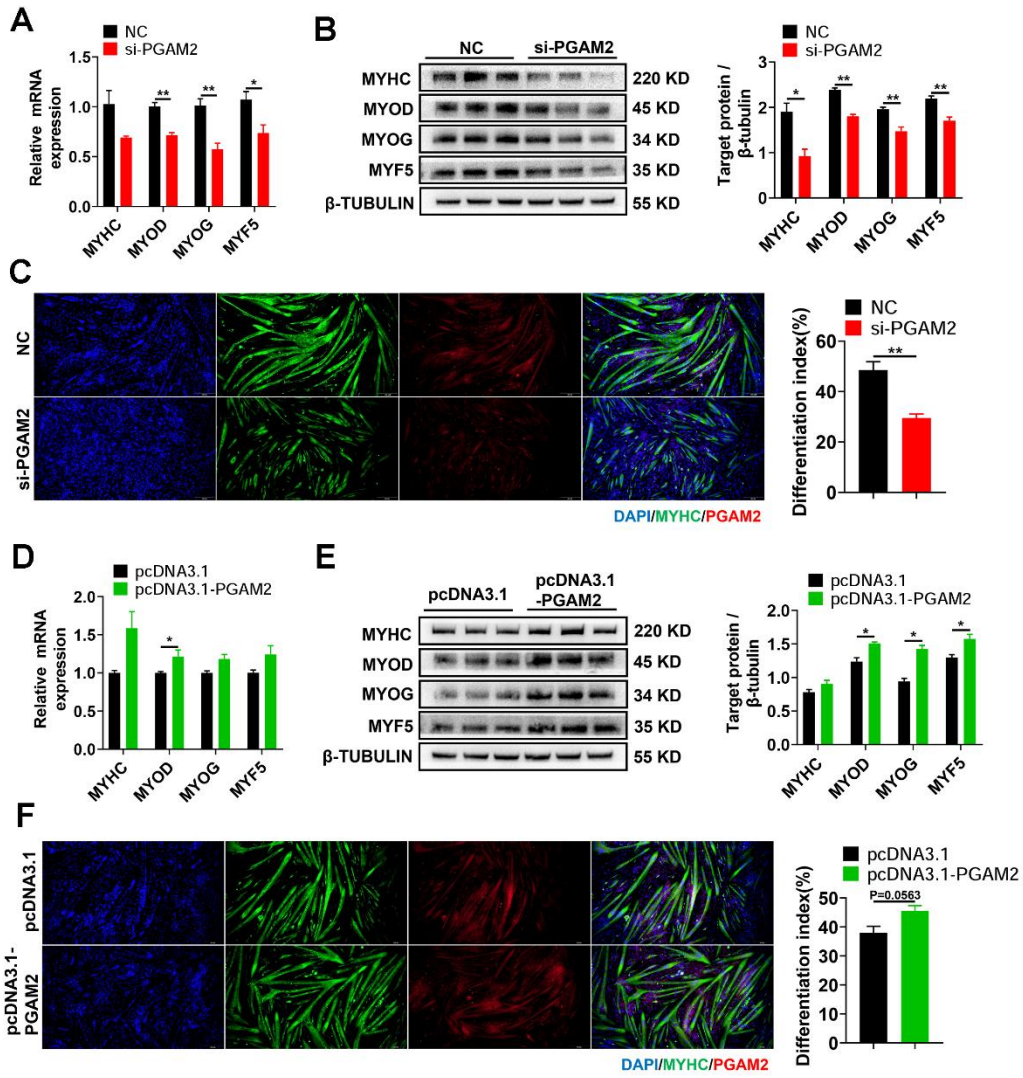

Fig. 4. *PGAM2* promotes the differentiation of porcine MuSCs. A. The mRNA expression levels of *MyHC*, *MyoD*, *MyoG*, and *Myf5* after knockdown of *PGAM2* as measured by qRT-PCR (n = 6). B. Protein levels of MyHC, MyoD, MyoG, and Myf5 after knockdown of *PGAM2* as analyzed by western blotting (n = 3). C. Immunofluorescence staining of MyHC after knockdown of *PGAM2* in MuSCs based on the differentiation index (n = 3). D. The mRNA expression levels of *MyHC*, *MyoD*, *MyoG*, and *Myf5* after overexpression of *PGAM2* as determined by qRT-PCR (n = 6). E. Protein levels of MyHC, MyoD, MyoG, and Myf5 after overexpression of

PGAM2 as measured by western blotting ($n = 3$). F. Immunofluorescence staining for MyHC after overexpression of *PGAM2* in MuSCs based on the differentiation index ($n = 3$). Results are mean ± SEM. Differences between means were detected by the independent samples *t*-tests (*$P < 0.05$; **$P < 0.01$).

3.4. PGAM2 promotes fast myofiber formation and inhibits mitochondrial biogenesis

As a component of the glycolytic pathway, *PGAM2* affects glucose utilization in skeletal muscle [22]. The *PGAM2* expression level was higher in LD (fast myofibers) than in SOL (slow myofibers) (Fig. 3A and Fig. 5A), which may be associated with the transformation of the skeletal myofibers. To assess this hypothesis, *PGAM2* was knocked down and overexpressed in porcine MuSCs. PGAM2 Knockdown significantly increased the expression levels of *MyHCI* and *MyHC IIa*, but significantly decreased the expression level of *MyHC IIb* (Fig. 5B). Knockdown of PGAM2 significantly promoted MyHC-slow protein expression (Fig. 5C). In contrast, overexpression of PGAM2 significantly increased the MyHC-fast protein level and decreased that of MyHC-slow (Fig. 5E).

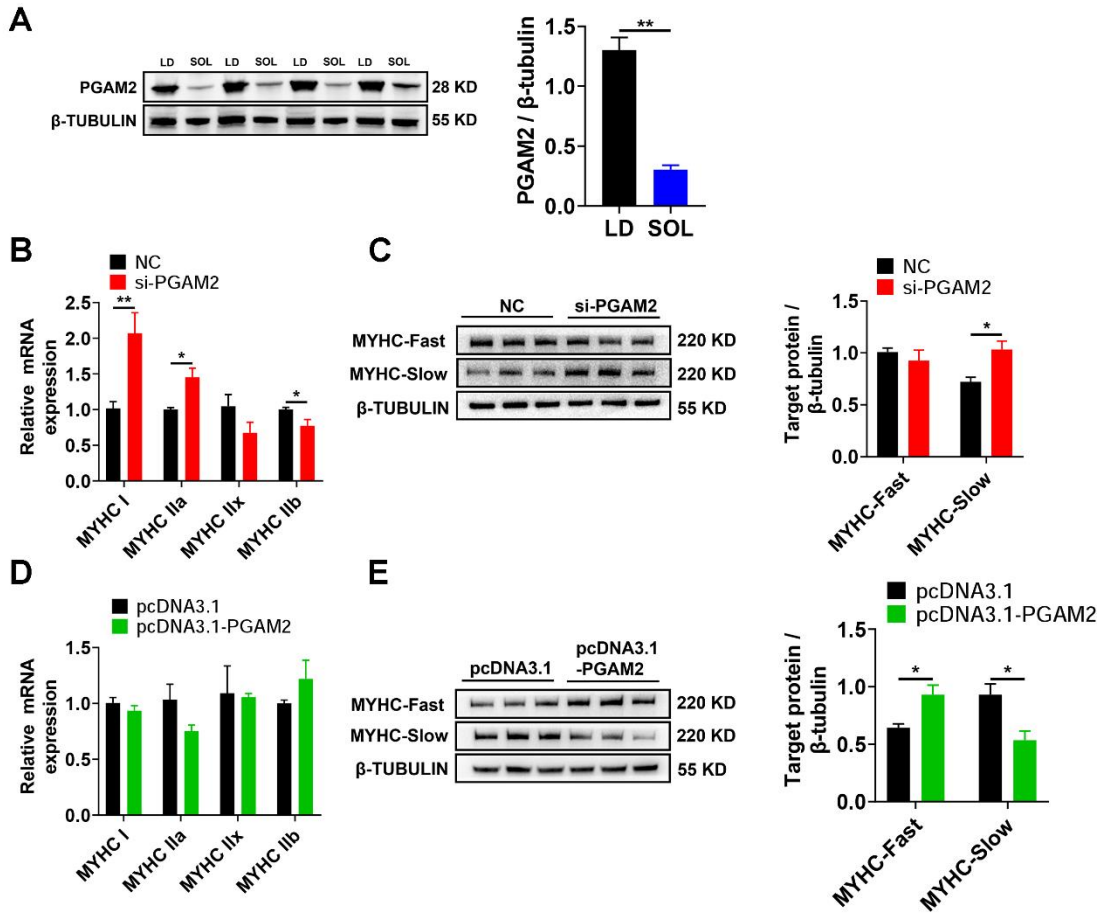

Fig. 5. *PGAM2* promotes fast muscle fiber formation. A. Protein levels of PGAM2 in the LD and SOL of 180-day-old pigs (n = 4). B. The mRNA expression levels of *MyHCI*, *MyHCIIa*, *MyHCIIx*, and *MyHCIIb* after knockdown of *PGAM2* as measured by qRT-PCR (n = 6). C. Protein levels of MyHC-slow and MyHC-fast after knockdown of *PGAM2* as analyzed by western blotting (n = 3). D. The mRNA expression levels of *MyHCI*, *MyHCIIa*, *MyHC IIx*, and *MyHC IIb* after overexpressing *PGAM2* as determined by qRT-PCR (n = 6). E. Protein levels of MyHC-slow and MyHC-fast after overexpression of *PGAM2* as measured by western blotting (n = 3). Results are mean ± SEM. Differences between means were detected by independent samples t-tests (*P < 0.05; **P < 0.01).

Next, we investigated whether *PGAM2* regulates myofiber turnover by affecting mitochondrial metabolism. Knockdown of *PGAM2* significantly increased the expression levels of the following marker genes compared to the control, related to mitochondrial biogenesis: *SDHB, NDUFB8, UQCRC2, NDUFA1, COX5A, CD36,* and *PGC-1α* (Fig. 6A); it also significantly increased the protein levels of the mitochondrial complex component NDUFB8 (Fig. 6B). Transmission electron microscopy revealed a significant increase in the number of mitochondria and the mitochondrial copy number (Fig. 6C, E). Mito-Tracker staining indicated a significant increase in the mitochondrial membrane potential (Fig. 6D). In contrast, overexpressing *PGAM2* significantly decreased the expression levels of these genes (Fig. 6F) and the protein levels of the mitochondrial complex components ATP5A and MTCO1 (Fig. 6G). The number of mitochondria (Fig. 6H), the mitochondrial copy number (Fig. 6J), and the membrane potential (Fig. 6I) increased significantly after overexpressing PGAM2. Therefore, *PGAM2* promotes the formation of fast myofibers by inhibiting mitochondrial function.

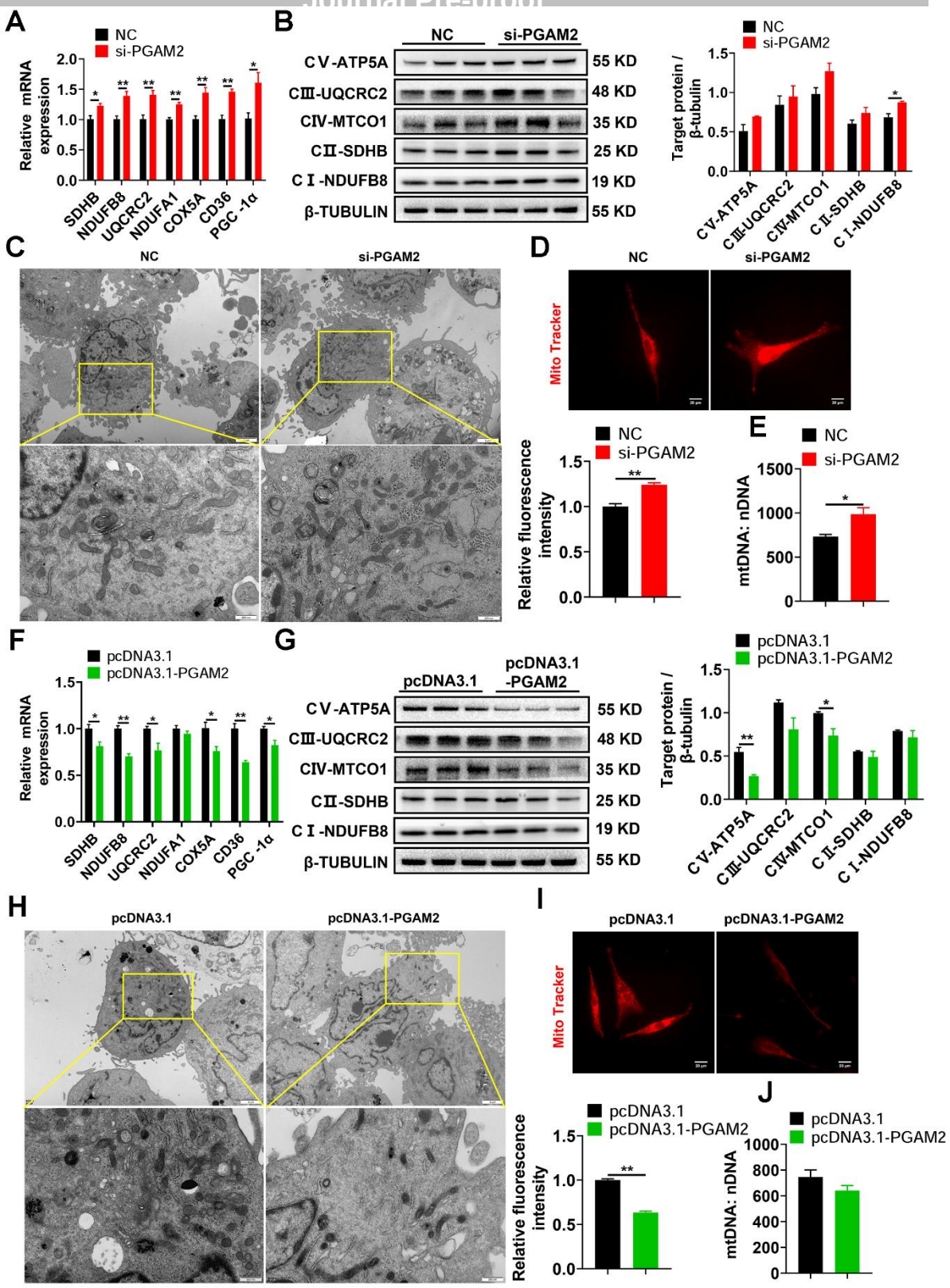

Fig. 6. PGAM2 inhibits mitochondrial biogenesis. A. The mRNA expression levels of genes related to mitochondrial biogenesis after knockdown of *PGAM2* as measured by qRT-PCR (n = 6). B. Protein levels of the mitochondrial complex components ATP5A, UQCRC2, MTCO1, SDHB, and NDUFB8 as analyzed by western blotting (n = 3). C. Mitochondrial morphology, size, and number in cells as determined by transmission electron microscopy. D. Mito-Tracker results showing the effects of knockdown of PGAM2 on the mitochondrial membrane potential (n = 3). E. Mitochondrial copy number in MuSCs (n = 3). F. The mRNA expression levels of genes related to mitochondrial biogenesis after overexpressing *PGAM2* as measured via qRT-PCR (n = 6). G.

Protein levels of the mitochondrial complex components ATP5A, UQCRC2, MTCO1, SDHB, and NDUFB8 as analyzed by western blotting (n = 3). H. Mitochondrial morphology, size, and number in cells as determined by transmission electron microscopy. I. Mito-Tracker results showing the effects of overexpressing PGAM2 on the mitochondrial membrane potential (n = 3). J. Mitochondrial copy number in MuSCs (n = 3). Results are mean ± SEM. Differences between means were detected by independent samples t-tests (*P < 0.05; **P < 0.01).

We further cross-treated the cells to verify the functional role between EPA and PGAM2. Adding EPA to proliferating cells significantly restored the protein levels of Ki67 and cyclin B in the *PGAM2* knockdown group compared to the NC+DMSO group (Fig. 7A). Similarly, adding EPA to differentiating cells significantly restored the protein levels of MyHC, MyoD, and MyoG and prevented the conversion of MyHC-fast to MyHC-slow in the knockdown group (Fig. 7B-C). Adding EPA also reduced the protein levels of the mitochondrial complex components ATP5A, UQCRC2, MTCO1, SDHB, and NDUFB8 in the knockdown group (Fig. 7D). Therefore, EPA regulates MuSCs by activating PGAM2.

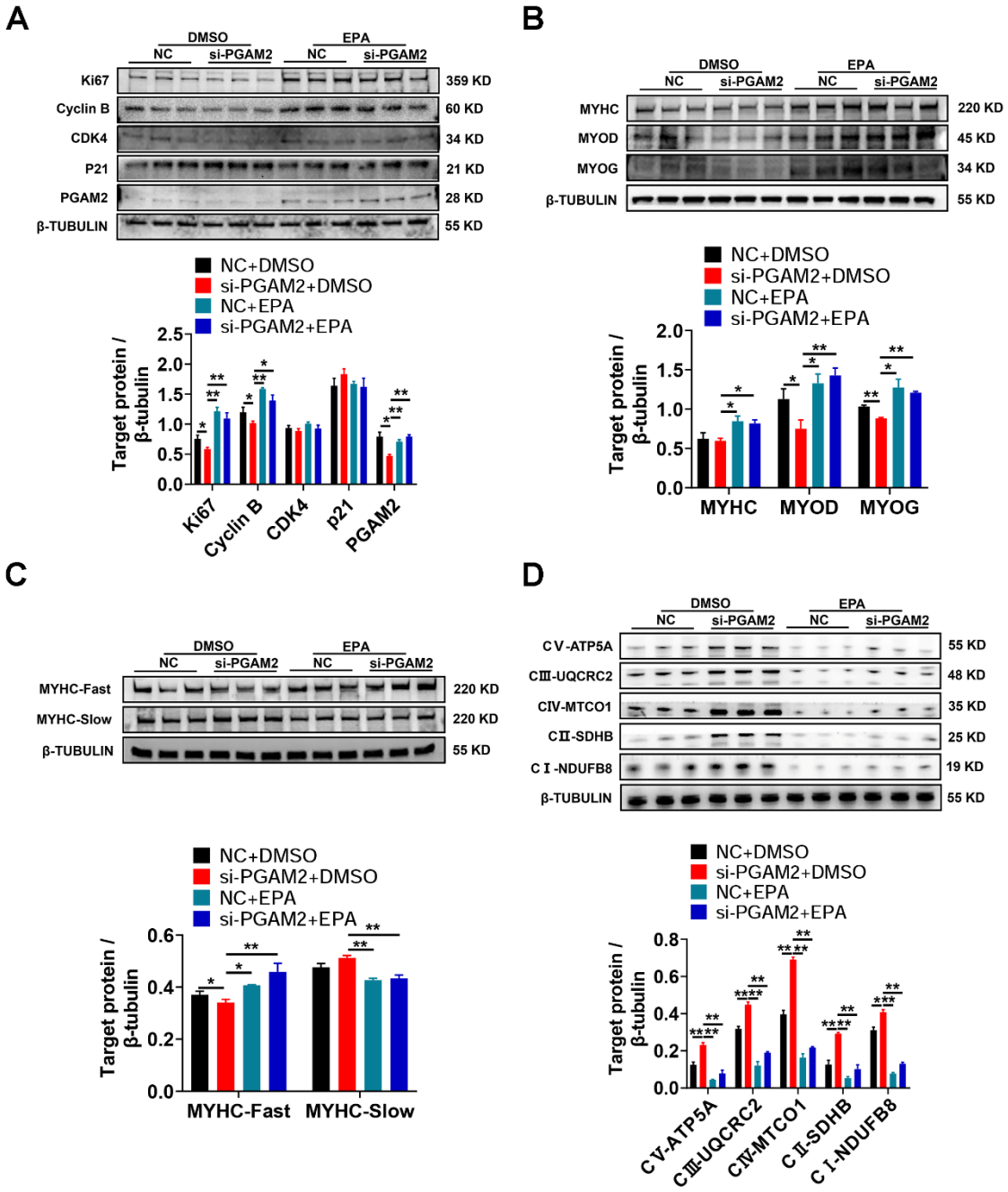

Fig. 7. Adding EPA restores the protein levels altered by PGAM2 knockdown. A. Protein levels of Ki67, cyclin B, CDK4 and p21 after adding of EPA and knockdown of *PGAM2* as measured by western blotting (n = 3). B. Protein levels of MyHC, MyoD, and MyoG (n = 3). C. Protein levels of MyHC-slow and MyHC-fast (n = 3). D. Protein levels of the mitochondrial complex components ATP5A, UQCRC2, MTCO1, SDHB, and NDUFB8 (n = 3). Results are mean ± SEM. ANOVA post-hoc analysis was performed using the Fisher's least significant difference test. (*P < 0.05; **P < 0.01).

3.5. Feeding EPA restores skeletal muscle function after PGAM2 knockdown

To investigate whether EPA regulates myofiber formation and transformation by targeting PGAM2, we fed EPA to 7-week-old mice in which *PGAM2* was knocked down in muscle (Fig. 8A). As results, no significant differences in body weight, muscle weight, visceral organ weight, adipose tissue inflammation, or lipid deposition were detected in the livers of the five groups

(Supplementary Fig. 1). Compared to the Control (CON) and AAV-NC+DMSO (ND), PGAM2 knockdown (SE) significantly decreased the diameter of the muscle fibers; however, EPA alone (NE) significantly increased their diameter. Furthermore, *PGAM2* knockdown significantly reduced the muscle fiber cross-sectional area in EPA-fed mice (NE), suggesting that *PGAM2* knockdown significantly attenuated the effect of EPA on muscle-fiber diameter (Fig. 8B-F). Immunofluorescence staining indicated no significant changes in the proportion of myofibers in the SOL. However, PGAM2 knockdown significantly increased the proportion of MYH7-positive myofibers in the GAS, and feeding EPA feeding significantly increased that of MYH4-positive myofibers. In addition, PGAM2 knockdown significantly attenuated the effect of EPA on MYH4-positive myofiber formation (Fig. 8G-I). Staining for succinate dehydrogenase (SDH) activity revealed that PGAM2 knockdown significantly attenuated the effect of EPA on muscle enzyme activity (Fig. 8J-K). The MYH7 protein level was significantly higher in the SD group and normal in the SE group; no significant differences in the protein levels of MYH2 or MYH1 were observed between the SD and SE groups. The MYH4 protein level was significantly lower in the SD group than in the ND group, significantly higher in the NE and SE groups, and slightly lower in the SE group, compared to the NE group (Fig. 8L).

The metabolic patterns of the muscle fibers determine their functions; fibers with a large proportion of slow-twitch muscle have better endurance and those with a large proportion of fast-twitch muscle have more explosive power. Exercise training assays in mice revealed no significant difference in endurance among the five groups (Fig. 8M-O). In contrast, the limb grip strength assays showed that the SD group had significantly fewer explosive muscle fibers. Transmission electron microscopy indicated no significant differences in mitochondrial size, morphology, or the inner ridge structure among the five groups (Fig. 8Q).

EPA activated PGAM2 and promoted the process of glycolysis, which, in turn, affected the formation of enzyme-type muscle fibers, increased the cross-sectional area of the muscle fibers, and improved the grip strength of the limbs of mice, but had no significant effect on the endurance of mice, which may be related to the lack of significant changes in the morphology, size, and number of mitochondria.

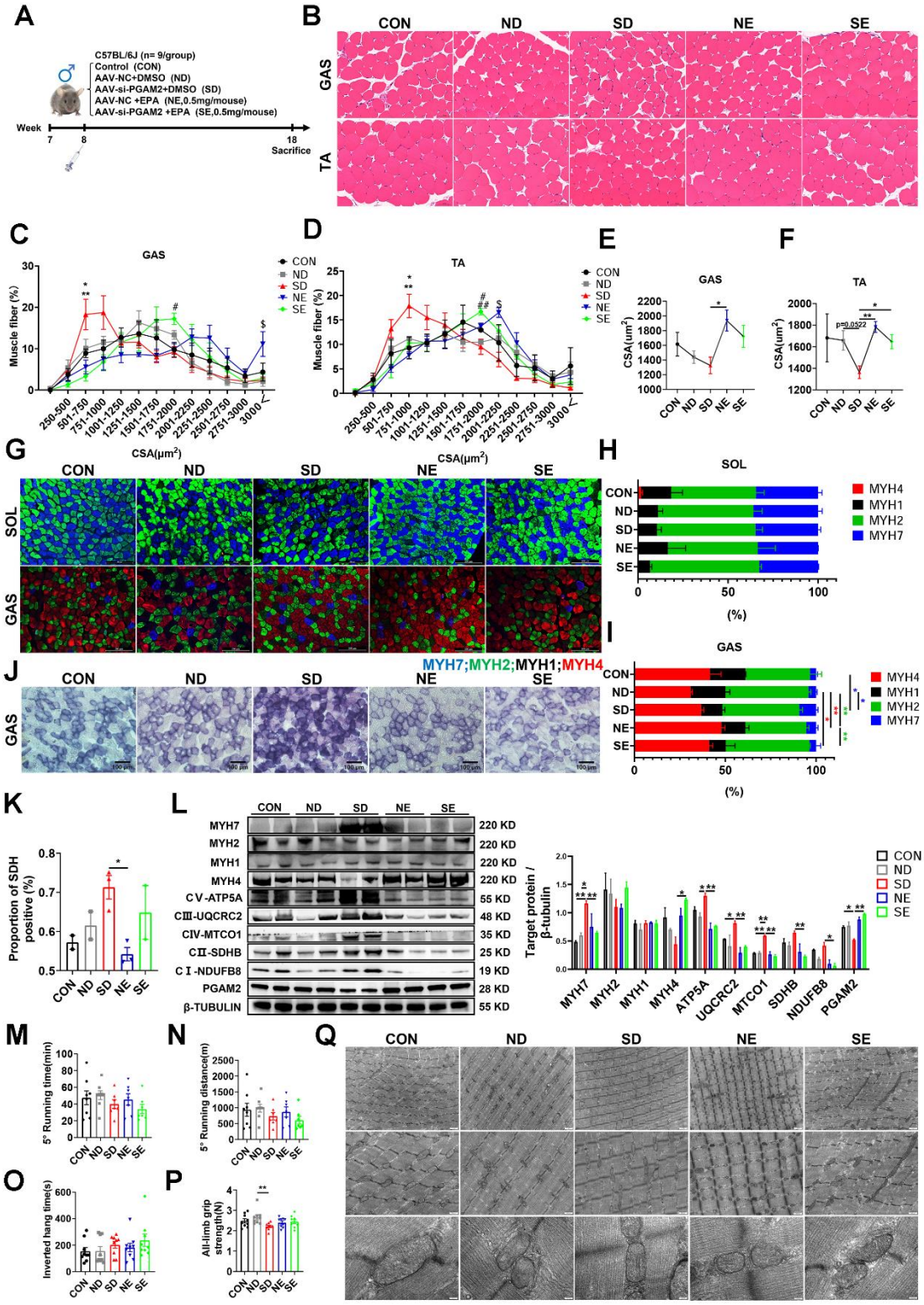

Fig. 8. Feeding of EPA restores skeletal muscle function after *PGAM2* knockdown. A. Schematic diagram the mouse feeding experiments. B-F. H&E-stained images and cross-sectional areas the GAS and TA muscles (GAS: *SD *vs*. NE; **SD *vs*. SE; # SE *vs*. CON, SE *vs*. SD, SE *vs*. NE; $ NE *vs*. ND, NE *vs*. SD; TA: *SD *vs*. CON; **SD *vs*. NE, SD *vs*. SE; # NE *vs*. SD; ## SE *vs*. ND, SE *vs*. SD; $ NE *vs*. SD; *n* = 3). G-I. The fiber types in the SOL and GAS were stained and enumerated. MYHC-I, MyHC-IIA, and MyHC-IIB were used as markers of type I, type IIa, and type IIb fibers, respectively (*n* = 3). J-K. Succinate dehydrogenase (SDH) staining (*n* = 3). L. Protein levels of MYH7, MYH2, MYH1, MYH4, ATP5A, UQCRC2, MTCO1, SDHB, and NDUFB8 as measured by western blotting (*n* = 2). M-P. Mouse 5° slope running time (M), 5° slope running distance (N), inversion time (O), and limb grip strength (P) (*n* = 9). Q. Transmission electron microscopy of mitochondrial morphology, size, and number. Results are mean ± SEM. ANOVA post-hoc analysis was performed using Fisher's

least significant difference test. (*$P < 0.05$; **$P < 0.01$).

3.6. EPA-activated PGAM2 modulates muscle function by PI3K/AKT signaling

To investigate how EPA-activated PGAM2 regulates skeletal muscle function, we conducted RNA-seq to screen the differentially expressed genes after EPA treatment or knockdown of PGAM2 in porcine MuSCs. The expression levels of 344 genes were altered in the EPA-treated group, including 153 upregulated and 191 downregulated genes. The expression of 97 genes was altered by PGAM2 knockdown, including 40 upregulated and 57 downregulated genes (Fig. 9A). KEGG pathway enrichment analysis revealed that both groups were highly enriched in the PI3K/AKT pathway (Fig 9B). Mammalian target of rapamycin complex 1 (mTORC1), a downstream substrate of the PI3K/AKT pathway, promotes protein synthesis by phosphorylating the key effectors S6 and 4EBP1 [35]. FOXO1 is a nuclear transcription factor whose phosphorylation in the cytoplasm regulates the PI3K/AKT pathway, and which is associated with myofiber formation [36, 37]. Thus, we evaluated the effects of EPA and PGAM2 on PI3K-AKT signaling in porcine MuSCs. The phosphorylation level of PI3K/AKT decreased significantly after PGAM2 knockdown, and those of the mTORC1 downstream substrates S6 and 4E-BP1 decreased significantly. Adding of EPA restored the phosphorylation levels of PI3K, AKT, S6, and 4E-BP1, and significantly decreased that of FOXO1 (Fig. 9C). PGAM2 activity s decreased significantly after PGAM2 knockdown but was significantly restored by EPA (Fig 9D). The i*n vivo* SD group showed significantly decreased phosphorylation of PI3K/AKT pathway components compared to the CON and ND groups, and the SE group significantly restored the phenotype to the SD group (Fig. 9E).

To verify that EPA regulates myogenesis and muscle fiber type transformation via the PI3K/AKT signaling pathway, we added a PI3K/AKT pathway inhibitor (GDC-0941) and EPA to porcine MuSCs and C2C12 cells, respectively. PI3K/AKT pathway activity was significantly inhibited and the FOXO1 phosphorylation level increased significantly in response to GDC-0941; adding EPA restored PI3K/AKT pathway activity (Fig. 9F-G). Similarly, the immunofluorescence results showed that the differentiation of MuSCs and C2C12 cells was significantly inhibited by GDC-0941, an effect reversed by EPA (Fig. 9H). Therefore, EPA regulates the proliferation, differentiation, and mitochondrial biogenesis of MuSCs via the PI3K/AKT signaling pathway, thereby regulating skeletal muscle function.

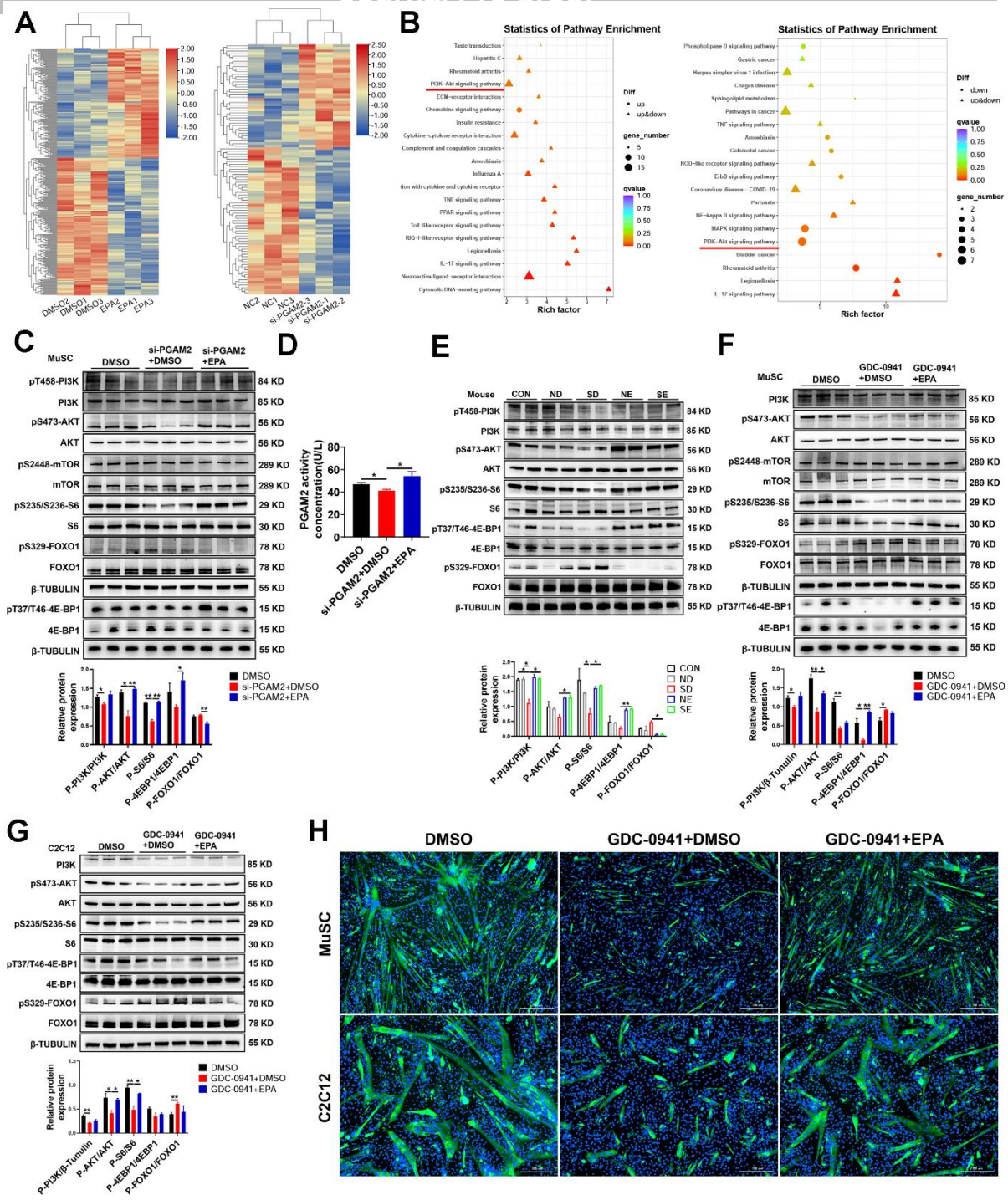

Fig. 9. EPA targets PGAM2 and activates the PI3K/AKT pathway. A. Heatmap of differentially expressed genes as determined via RNA-seq. B. KEGG pathway analysis of differentially expressed genes. C. The MuSC protein levels of the components of the PI3K/AKT pathway after EPA treatment and *PGAM2* interference were measured by western blotting (n = 3). D. ELISA for the effect of EPA after *PGAM2* knockdown (n = 3). E. Effect of EPA on the protein levels of components in the PI3K/AKT pathway after knockdown as analyzed by western blotting (n = 2). F-G. Effects of EPA and a PI3K/AKT pathway inhibitor (GDC-0941) on the protein levels of components of the PI3K/AKT pathway in MuSCs (F) and C2C12 cells (G) as determined by western blotting (n = 3). H. Immunofluorescence staining of MyHC to evaluate the differentiation of MuSCs and C2C12 cells. Results are mean ± SEM. ANOVA post-hoc analysis was performed using Fisher's least significant difference test. (*P < 0.05; **P < 0.01).

4. Discussion

Skeletal muscle is important in energy metabolism, movement, and health and is a significant source of protein. A change in muscle fiber composition affects the metabolic capacity of muscle as well as its homeostasis, size, and quality. EPA, the major n-3 PUFA in fish oil, improves glucose uptake and protein synthesis in skeletal muscle [38, 39] and promotes its growth [40]. However, how it affects muscle growth is unclear. Here, we report that EPA promoted the proliferation and differentiation of porcine MuSCs. In addition, it promotes the formation of fast myofibers and inhibits the formation of slow myofibers, mitochondrial biosynthesis by increasing the levels of components of the mitochondrial complex, and muscle hypertrophy. It also alleviates muscle atrophy [41, 42], suggesting that it enhances muscle growth and metabolism.

The mechanism by which EPA affects muscle growth and muscle fiber metabolism is unclear. PUFAs target protein receptors, affecting their stability, and participate in a variety of signaling pathways. For example, DHA inhibits fibroblast activation by targeting p38/ET-1. PGAM2 is a key enzyme in the glycolytic pathway that mediates the conversion of 2-PG into 3-PG. Small molecule targeting prediction and experimental verification revealed that EPA targets PGAM2 and increases its level and activity. However, we detected strong interactions between EPA and ARG-86, ASP-157, GLU-148, GLU-153, and ARG-161 in PGAM2 in molecular docking simulations, which we could not verify and limited our experiment. Mutations at one site can change the structure of the entire protein and affect its activity, thus affecting the interaction between EPA and PGAM2. We have verified its binding ability through CETSA, but the specific site of action needs to be further explored. PGAM2 is localized to the cytoplasm and nucleus and is involved in glycolysis. We showed here that it promoted the formation of glycolytic muscle fibers, inhibited oxidative phosphorylation of mitochondria, and affected the expression of components of the mitochondrial complex. Therefore, we verified that EPA increases the PGAM2 level and activity by targeting PGAM2, and inhibits mitochondrial biogenesis and oxidative phosphorylation, leading to the generation of fast-oxidizing myofibers. Consistent with this hypothesis, EPA significantly mitigated the effect of *PGAM2* knockdown on the proportions of myofiber types and mitochondrial metabolism by significantly increasing PGAM2 activity. However, fatty acids are oxidatively metabolized through the tricarboxylic acid (TCA) cycle to supply energy, and enhancing the TCA cycle promotes mitochondrial biogenesis, which produces large quantities of ATP, so that

most of the fatty acids that enter the cell activate the TCA cycle, and glycolysis is weakened, resulting in large quantities of energy being produced [43]. When EPA enters the cell, it promotes glycolysis by activating PGAM2. However, as a free fatty acid, the effect of EPA on the TCA cycle was not significant, suggesting that EPA acts as a PGAM2 activator much more than its fatty acid structure. Thus, the balance between EPA and glycolysis and fatty acid oxidation remains to be determined.

Moreover, the RNA-seq analysis showed that EPA and PGAM2 share downstream target genes and signaling pathways, including those of PI3K-AKT, TNF, and IL-17. The PI3K/AKT pathway determines cell fate and plays an important role in cell proliferation, differentiation, and myofiber-type transformation [44], and phosphorylation of AKT directly modulates cell cycle proteins to affect cell proliferation. Our results show that interfering with PGAM2 decreased PGAM2 activity, thereby inhibiting the phosphorylation of components of the PI3K-AKT signaling pathway and activating the FOXO1 transcription factor. PGAM2 activity was restored by adding EPA, and the phosphorylation levels of the PI3K/AKT signaling pathway components were restored. FOXO1 regulates skeletal muscle energy homeostasis via glycolysis and mitochondrial metabolism [36]. FOXO1 regulates carbohydrate catabolism in skeletal muscle during fasting [45] and transgenic FOXO1 mice have reduced muscle volume and weight and a decreased proportion of MYHC type I muscle fibers [46]. Changes in ATP levels during glycolysis affect PI3K-Akt-FOXO1 signaling [47]. In this study, activation of the PI3K/AKT signaling pathway decreased FOXO1 phosphorylation and significantly inhibited mitochondrial metabolism. PGAM2 knockdown inhibits glycolysis, decreases the phosphorylation of PI3K/AKT signaling pathway components, and activates the phosphorylation of FOXO1 and mitochondrial metabolism. The result is a change in the balance between glycolysis and oxidative phosphorylation in favor of the latter, resulting in the transformation of glycolytic fibers into rapidly oxidizing muscle fibers. It has also been previously reported that glycolysis activates the PI3K/AKT/FOXO1 signaling pathway [48][49], which is consistent with our findings. However, PGAM2 is expressed in both the cytoplasm and the nucleus, and activation of PGAM2 in the cytoplasm promotes the expression of the PI3K/AKT signaling pathway, whereas translocation of PGAM2 to the nucleus requires mediation of the cytoplasmic PI3K/AKT signaling pathway [50]; thus, further explorations is needed to determine the translocation of PGAM2 to the nucleus as well as for the roles of PGAM2 in the nucleus versus the cytoplasm.

5. Conclusion

Consumption of fish oil is beneficial to skeletal muscle health. We determined that EPA, the main component in fish oil, promotes the proliferation and differentiation of porcine skeletal muscle satellite cells and the formation of rapidly oxidizing myofibers. Through molecular docking and other experiments, EPA increased the expression level and activity of PGAM2 by targeting PGAM2, a key enzyme in glycolysis, and the increased PGAM2 activity promoted glycolysis, which activated PI3K-AKT signaling, promotes the proliferation and differentiation of porcine skeletal muscle satellite cells, and promoted the synthesis of proteins, as well as inhibited the transcriptional activity of FOXO1, leading to the formation of rapidly oxidizing myofibers. Our results will help us understand the molecular regulatory network during muscle development, provide a basis for selecting nutritional supplements for muscle injury or muscle disease, and provide a theoretical basis for selecting of feed additives for growing and fattening pigs.

Author contributions

Chenchen Li: experimental part and manuscript writing; **Haigang Cao**: manuscript revision; **Yingchun Ren** and **Jinrui Jia**: data reduction; **Gongshe Yang**: experimental design; **Jianjun Jin**: Data analysis and experimental design; **Xin'e Shi**: funding is provided and ideas are tested.

Funding statement

This work was supported by National Key Research and Development Program of China (2021YFF1000602) to Xin E Shi. The funder had no role in study design, data collection and analysis, decision to publish, or preparation of the manuscript.

Declaration of interest statement

The authors declare that they have no known competing financial interests or personal relationships that could have appeared to influence the work reported in this paper.

Acknowledgments

The authors would like to thank Life Science Research Core Services of Northwest A&F University for image analysis.

References

[1] M.N. Wosczyna, T.A. Rando, A Muscle Stem Cell Support Group: Coordinated Cellular Responses in Muscle Regeneration, Dev. Cell. 46 (2018) 135-143.https://doi.org/10.1016/j.devcel.2018.06.018.

[2] N. Motohashi, A. Asakura, Muscle satellite cell heterogeneity and self-renewal, Front. Cell. Dev. Biol. 2 (2014) 1.https://doi.org/10.3389/fcell.2014.00001.

[3] S. Bataille, N. McKay, L. Koppe, A. Beau, B. Benoit, M. Bartoli, N. Da Silva, S. Poitevin, J. Aniort, R. Chermiti, S. Burtey, L. Dou, Indoxyl sulfate inhibits muscle cell differentiation via Myf6/MRF4 and MYH2 downregulation, Nephrology, dialysis, transplantation : official publication of the European Dialysis and Transplant Association - European Renal Association DOI 10.1093/ndt/gfad123(2023).https://doi.org/10.1093/ndt/gfad123.

[4] B.M. Cleveland, G. Gao, T.D. Leeds, Transcriptomic Response to Selective Breeding for Fast Growth in Rainbow Trout (Oncorhynchus mykiss), Mar Biotechnol (NY) 22 (2020) 539-550.https://doi.org/10.1007/s10126-020-09974-3.

[5] M. Buckingham, Myogenic progenitor cells and skeletal myogenesis in vertebrates, Curr. Opin. Genet. Dev. 16 (2006) 525-532.https://doi.org/10.1016/j.gde.2006.08.008.

[6] S. Schiaffino, C. Reggiani, Fiber types in mammalian skeletal muscles, Physiol. Rev. 91 (2011) 1447-1531.https://doi.org/10.1152/physrev.00031.2010.

[7] A. Listrat, B. Lebret, I. Louveau, T. Astruc, M. Bonnet, L. Lefaucheur, B. Picard, J. Bugeon, How Muscle Structure and Composition Influence Meat and Flesh Quality, ScientificWorldJournal 2016 (2016) 3182746.https://doi.org/10.1155/2016/3182746.

[8] B. Picard, M. Gagaoua, Muscle Fiber Properties in Cattle and Their Relationships with Meat Qualities: An Overview, J. Agric. Food Chem. 68 (2020) 6021-6039.https://doi.org/10.1021/acs.jafc.0c02086.

[9] P. Koutakis, D.J. Weiss, D. Miserlis, V.K. Shostrom, E. Papoutsi, D.M. Ha, L.A. Carpenter, R.D. McComb, G.P. Casale, Pipinos, II, Oxidative damage in the gastrocnemius of patients with peripheral artery disease is myofiber type selective, Redox Biol. 2 (2014) 921-928.https://doi.org/10.1016/j.redox.2014.07.002.

[10] M. Gagaoua, B. Picard, Current Advances in Meat Nutritional, Sensory and Physical Quality Improvement, Foods. 9 (2020).https://doi.org/10.3390/foods9030321.

[11] J. Zhang, J. Li, Y. Liu, R. Liang, Y. Mao, X. Yang, Y. Zhang, L. Zhu, Effect of resveratrol on skeletal slow-twitch muscle fiber expression via AMPK/PGC-1α signaling pathway in bovine myotubes, Meat Sci. 204 (2023) 109287.https://doi.org/10.1016/j.meatsci.2023.109287.

[12] G.I. Smith, S. Julliand, D.N. Reeds, D.R. Sinacore, S. Klein, B. Mittendorfer, Fish oil-derived n-3 PUFA therapy increases muscle mass and function in healthy older adults, Am. J. Clin. Nutr. 102 (2015) 115-122.https://doi.org/10.3945/ajcn.114.105833.

[13] G. Gortan Cappellari, A. Semolic, G. Ruozi, D. Barbetta, F. Bortolotti, P. Vinci, M. Zanetti, R.H. Mak, G. Garibotto, M. Giacca, R. Barazzoni, n-3 PUFA dietary lipid replacement normalizes muscle mitochondrial function and oxidative stress through enhanced tissue mitophagy and protects from muscle wasting in experimental kidney disease, Metabolism 133

(2022) 155242.https://doi.org/10.1016/j.metabol.2022.155242.
[14] D.K. Gessner, B. Gröne, A. Couturier, S. Rosenbaum, S. Hillen, S. Becker, G. Erhardt, G. Reiner, R. Ringseis, K. Eder, Dietary Fish Oil Inhibits Pro-Inflammatory and ER Stress Signalling Pathways in the Liver of Sows during Lactation, PloS one. 10 (2015) e0137684.https://doi.org/10.1371/journal.pone.0137684.
[15] E. Ochi, Y. Tsuchiya, Eicosapentaenoic Acid (EPA) and Docosahexaenoic Acid (DHA) in Muscle Damage and Function, Nutrients. 10 (2018).https://doi.org/10.3390/nu10050552.
[16] J.M. Budd, B. Hucik, C. Wang, A.N. King, O. Sarr, M.T. Nakamura, E. Harasim-Symbor, A. Chabowski, D.J. Dyck, D.M. Mutch, A reduction of skeletal muscle DHA content does not result in impaired whole body glucose tolerance or skeletal muscle basal insulin signaling in otherwise healthy mice, Am. J. Physiol. Endocrinol. Metab. 324 (2023) E241-e250.https://doi.org/10.1152/ajpendo.00308.2022.
[17] C. McGlory, P.C. Calder, E.A. Nunes, The Influence of Omega-3 Fatty Acids on Skeletal Muscle Protein Turnover in Health, Disuse, and Disease, Front. Nutr. 6 (2019) 144.https://doi.org/10.3389/fnut.2019.00144.
[18] P. Magee, S. Pearson, J. Allen, The omega-3 fatty acid, eicosapentaenoic acid (EPA), prevents the damaging effects of tumour necrosis factor (TNF)-alpha during murine skeletal muscle cell differentiation, Lipids Health Dis. 7 (2008) 24.https://doi.org/10.1186/1476-511x-7-24.
[19] M.A. Tarnopolsky, Myopathies Related to Glycogen Metabolism Disorders, Neurotherapeutics. 15 (2018) 915-927.https://doi.org/10.1007/s13311-018-00684-2.
[20] Q. Gang, C. Bettencourt, S. Brady, J.L. Holton, E.G. Healy, J. McConville, P.J. Morrison, M. Ripolone, R. Violano, M. Sciacco, M. Moggio, M. Mora, R. Mantegazza, S. Zanotti, Z. Wang, Y. Yuan, W.W. Liu, D. Beeson, M. Hanna, H. Houlden, Genetic defects are common in myopathies with tubular aggregates, Ann. Clin. Transl. Neurol. 9 (2022) 4-15.https://doi.org/10.1002/acn3.51477.
[21] Y.R. Li, J.D. Chen, Y.Y. Zhu, J.T. Li, G.Z. Jin, R.M. Jin, Evaluation of nuclear PGAM2 value in hepatocellular carcinoma prognosis, Anti-cancer drugs 33 (2022) e500-e506.https://doi.org/10.1097/cad.0000000000001150.
[22] H. Qiu, S. Zhao, X. Xu, M. Yerle, B. Liu, Assignment and expression patterns of porcine muscle-specific isoform of phosphoglycerate mutase gene, J. Genet. Genomics. 35 (2008) 257-260.https://doi.org/10.1016/s1673-8527(08)60036-3.
[23] L. Fontanesi, R. Davoli, L. Nanni Costa, F. Beretti, E. Scotti, M. Tazzoli, F. Tassone, M. Colombo, L. Buttazzoni, V. Russo, Investigation of candidate genes for glycolytic potential of porcine skeletal muscle: Association with meat quality and production traits in Italian Large White pigs, Meat Sci. 80 (2008) 780-787.https://doi.org/10.1016/j.meatsci.2008.03.022.
[24] D.S. Antonelo, J.F.M. Gómez, S.L. Silva, M. Beline, X. Zhang, Y. Wang, B. Pavan, L.A. Koulicoff, A.F. Rosa, R.S. Goulart, S. Li, D.E. Gerrard, S.P. Suman, M. Wes Schilling, J.C.C. Balieiro, Proteome basis for the biological variations in color and tenderness of longissimus thoracis muscle from beef cattle differing in growth rate and feeding regime, Food Res. Int. 153 (2022) 110947.https://doi.org/10.1016/j.foodres.2022.110947.
[25] H. Cao, T. Du, C. Li, L. Wu, J. Liu, Y. Guo, X. Li, G. Yang, J. Jin, X. Shi, MicroRNA-668-3p inhibits myoblast proliferation and differentiation by targeting Appl1, BMC Genomics. 24 (2023) 415.https://doi.org/10.1186/s12864-023-09431-0.
[26] C. Wang, F. Yue, S. Kuang, Muscle Histology Characterization Using H&E Staining and Muscle Fiber Type Classification Using Immunofluorescence Staining, Bio. Protoc. 7 (2017).https://doi.org/10.21769/BioProtoc.2279.

[27] P. Tizro, C. Choi, N. Khanlou, Sample Preparation for Transmission Electron Microscopy, Methods. Mol. Biol. 1897 (2019) 417-424.https://doi.org/10.1007/978-1-4939-8935-5_33.
[28] Y. Wu, Y. He, H. Luo, T. Jin, F. He, AIEE-Active Flavones as a Promising Tool for the Real-Time Tracking of Uptake and Distribution in Live Zebrafish, Int. J. Mol. Sci. 24 (2023).https://doi.org/10.3390/ijms241210183.
[29] A. Baig, H. Srinivasan, SARS-CoV-2 Inhibitors from Nigella Sativa, Appl. Biochem. Biotechnol. 194 (2022) 1051-1090.https://doi.org/10.1007/s12010-021-03790-8.
[30] K. Chen, Y. Zheng, J.A. Wei, H. Ouyang, X. Huang, F. Zhang, C.S.W. Lai, C. Ren, K.F. So, L. Zhang, Exercise training improves motor skill learning via selective activation of mTOR, Sci. Adv. 5 (2019) eaaw1888.https://doi.org/10.1126/sciadv.aaw1888.
[31] Y. Yue, Y. Yue, Z. Fan, Y. Meng, C. Wen, Y. An, Y. Yao, X. Li, The long noncoding RNA lnc-H19 is important for endurance exercise by maintaining slow muscle fiber types, J. Biol. Chem. 299 (2023) 105281.https://doi.org/10.1016/j.jbc.2023.105281.
[32] R. Jafari, H. Almqvist, H. Axelsson, M. Ignatushchenko, T. Lundbäck, P. Nordlund, D. Martinez Molina, The cellular thermal shift assay for evaluating drug target interactions in cells, Nat. Protoc. 9 (2014) 2100-2122.https://doi.org/10.1038/nprot.2014.138.
[33] M.R. Jackman, W.T. Willis, Characteristics of mitochondria isolated from type I and type IIb skeletal muscle, Am. J. Physiol. 270 (1996) C673-678.https://doi.org/10.1152/ajpcell.1996.270.2.C673.
[34] P.B. Katare, A. Dalmao-Fernandez, A.M. Mengeste, H. Hamarsland, S. Ellefsen, H.G. Bakke, E.T. Kase, G.H. Thoresen, A.C. Rustan, Energy metabolism in skeletal muscle cells from donors with different body mass index, Front. Physiol. 13 (2022) 982842.https://doi.org/10.3389/fphys.2022.982842.
[35] C.L. Jin, Z.M. Zhang, Z.W. Song, C.Q. Gao, H.C. Yan, X.Q. Wang, mTORC1-Mediated Satellite Cell Differentiation Is Required for Lysine-Induced Skeletal Muscle Growth, J. Agric. Food Chem. 68 (2020) 4884-4892.https://doi.org/10.1021/acs.jafc.0c01275.
[36] A.M. Sanchez, R.B. Candau, H. Bernardi, FoxO transcription factors: their roles in the maintenance of skeletal muscle homeostasis, Cell. Mol. Life. Sci. 71 (2014) 1657-1671.https://doi.org/10.1007/s00018-013-1513-z.
[37] Z. Gombos, E. Koltai, F. Torma, P. Bakonyi, A. Kolonics, D. Aczel, T. Ditroi, P. Nagy, T. Kawamura, Z. Radak, Hypertrophy of Rat Skeletal Muscle Is Associated with Increased SIRT1/Akt/mTOR/S6 and Suppressed Sestrin2/SIRT3/FOXO1 Levels, Int. J. Mol. Sci. 22 (2021).https://doi.org/10.3390/ijms22147588.
[38] G. Katsnelson, R.B. Ceddia, Docosahexaenoic and eicosapentaenoic fatty acids differentially regulate glucose and fatty acid metabolism in L6 rat skeletal muscle cells, Am. J. Physiol. Cell. Physiol. 319 (2020) C1120-c1129.https://doi.org/10.1152/ajpcell.00304.2020.
[39] S. Jeromson, I. Mackenzie, M.K. Doherty, P.D. Whitfield, G. Bell, J. Dick, A. Shaw, F.V. Rao, S.P. Ashcroft, A. Philp, S.D.R. Galloway, I. Gallagher, D.L. Hamilton, Lipid remodeling and an altered membrane-associated proteome may drive the differential effects of EPA and DHA treatment on skeletal muscle glucose uptake and protein accretion, Am. J. Physiol. Endocrinol. Metab. 314 (2018) E605-e619.https://doi.org/10.1152/ajpendo.00438.2015.
[40] A. Saini, A.P. Sharples, N. Al-Shanti, C.E. Stewart, Omega-3 fatty acid EPA improves regenerative capacity of mouse skeletal muscle cells exposed to saturated fat and inflammation, Biogerontology. 18 (2017) 109-129.https://doi.org/10.1007/s10522-016-9667-3.
[41] Y. Ikeno, M. Inomata, Y. Tsukimura, Y. Suzuki, H. Takeuchi, Y. Harada, R. Kon, N. Ikarashi, Y. Chiba, T. Yamada, J. Kamei, H. Sakai, Eicosapentaenoic acid suppresses cisplatin-induced muscle atrophy by attenuating the up-regulated gene expression of

ubiquitin, J. Nutr. Biochem. 103 (2022) 108953.https://doi.org/10.1016/j.jnutbio.2022.108953.
[42] S. Siriguleng, T. Koike, Y. Natsume, H. Jiang, L. Mu, Y. Oshida, Eicosapentaenoic acid enhances skeletal muscle hypertrophy without altering the protein anabolic signaling pathway, Physiol. Res. 70 (2021) 55-65.https://doi.org/10.33549/physiolres.934534.
[43] F.J. Weisel, S.J. Mullett, R.A. Elsner, A.V. Menk, N. Trivedi, W. Luo, D. Wikenheiser, W.F. Hawse, M. Chikina, S. Smita, L.J. Conter, S.M. Joachim, S.G. Wendell, M.J. Jurczak, T.H. Winkler, G.M. Delgoffe, M.J. Shlomchik, Germinal center B cells selectively oxidize fatty acids for energy while conducting minimal glycolysis, Nat. Immunol. 21 (2020) 331-342.https://doi.org/10.1038/s41590-020-0598-4.
[44] L. Chen, X. Li, Y. Deng, J. Chen, M. Huang, F. Zhu, Z. Gao, L. Wu, Q. Hong, Z. Feng, G. Cai, X. Sun, X. Bai, X. Chen, The PI3K-Akt-mTOR pathway mediates renal pericyte-myofibroblast transition by enhancing glycolysis through HKII, J. Transl. Med. 21 (2023) 323.https://doi.org/10.1186/s12967-023-04167-7.
[45] S. Kousteni, Fox01, the transcriptional chief of staff of energy metabolism, Bone. 50 (2012) 437-443.https://doi.org/10.1016/j.bone.2011.06.034.
[46] Y. Kamei, S. Miura, M. Suzuki, Y. Kai, J. Mizukami, T. Taniguchi, K. Mochida, T. Hata, J. Matsuda, H. Aburatani, I. Nishino, O. Ezaki, Skeletal muscle FOXO1 (FKHR) transgenic mice have less skeletal muscle mass, down-regulated Type I (slow twitch/red muscle) fiber genes, and impaired glycemic control, J. Biol. Chem. 279 (2004) 41114-41123.https://doi.org/10.1074/jbc.M400674200.
[47] K. Xu, N. Yin, M. Peng, E.G. Stamatiades, A. Shyu, P. Li, X. Zhang, M.H. Do, Z. Wang, K.J. Capistrano, C. Chou, A.G. Levine, A.Y. Rudensky, M.O. Li, Glycolysis fuels phosphoinositide 3-kinase signaling to bolster T cell immunity, Science. 371 (2021) 405-410.https://doi.org/10.1126/science.abb2683.
[48] X. Peng, H. Li, L. Zhu, S. Zhao, Z. Li, S. Li, DongtingWu, J. Chen, S. Zheng, W. Su, Single-cell sequencing of the retina shows that LDHA regulates pathogenesis of autoimmune uveitis, J. Autoimmun. 143 (2023) 103160.https://doi.org/10.1016/j.jaut.2023.103160.
[49] K. Xu, N. Yin, M. Peng, E.G. Stamatiades, S. Chhangawala, A. Shyu, P. Li, X. Zhang, M.H. Do, K.J. Capistrano, C. Chou, C.S. Leslie, M.O. Li, Glycolytic ATP fuels phosphoinositide 3-kinase signaling to support effector T helper 17 cell responses, Immunity. 54 (2021) 976-987.e977.https://doi.org/10.1016/j.immuni.2021.04.008.
[50] J. Wiśniewski, J. Barciszewski, J. Turlik, K. Baran, P. Duda, M. Jaskolski, D. Rakus, High-Resolution Crystal Structure of Muscle Phosphoglycerate Mutase Provides Insight into Its Nuclear Import and Role, Int. J. Mol. Sci. 23 (2022).https://doi.org/10.3390/ijms232113198.

ABBREVIATIONS

Eicosapentaenoic acid (EPA); phosphoglycerate mutase 2 (PGAM2); skeletal muscle satellite cell (MuSC); myosin heavy chain (MyHC); RNA sequencing (RNA-seq); mammalian target of rapamycin complex 1 (mTORC1); paired box 7 (Pax7); peroxisome receptor proliferation-activated receptor gamma coactivator-1α (PGC-1α); ATP synthase subunit alpha (ATP5A); cytochrome b-c1 complex subunit 2 (UQCRC2); cytochrome c oxidase subunit 1 (MTCO1); succinate dehydrogenase iron-sulfur subunit (SDHB); NADH dehydrogenase [ubiquinone] 1

beta subcomplex subunit 8 (NDUFB8); acetate dehydrogenase (LDHA); pyruvate kinase (PKM); phosphoglycerate kinase 1 (PGK1); 3-phosphoglycerate (3-PG); 2-phosphoglycerate (2-PG); longissimus dorsi (LD); soleus (SOL); tibialis anterior (TA); gastrocnemius (GAS); phosphoglycerate mutase 1 (PGAM1); tricarboxylic acid (TCA)

Supplementary Fig. 1

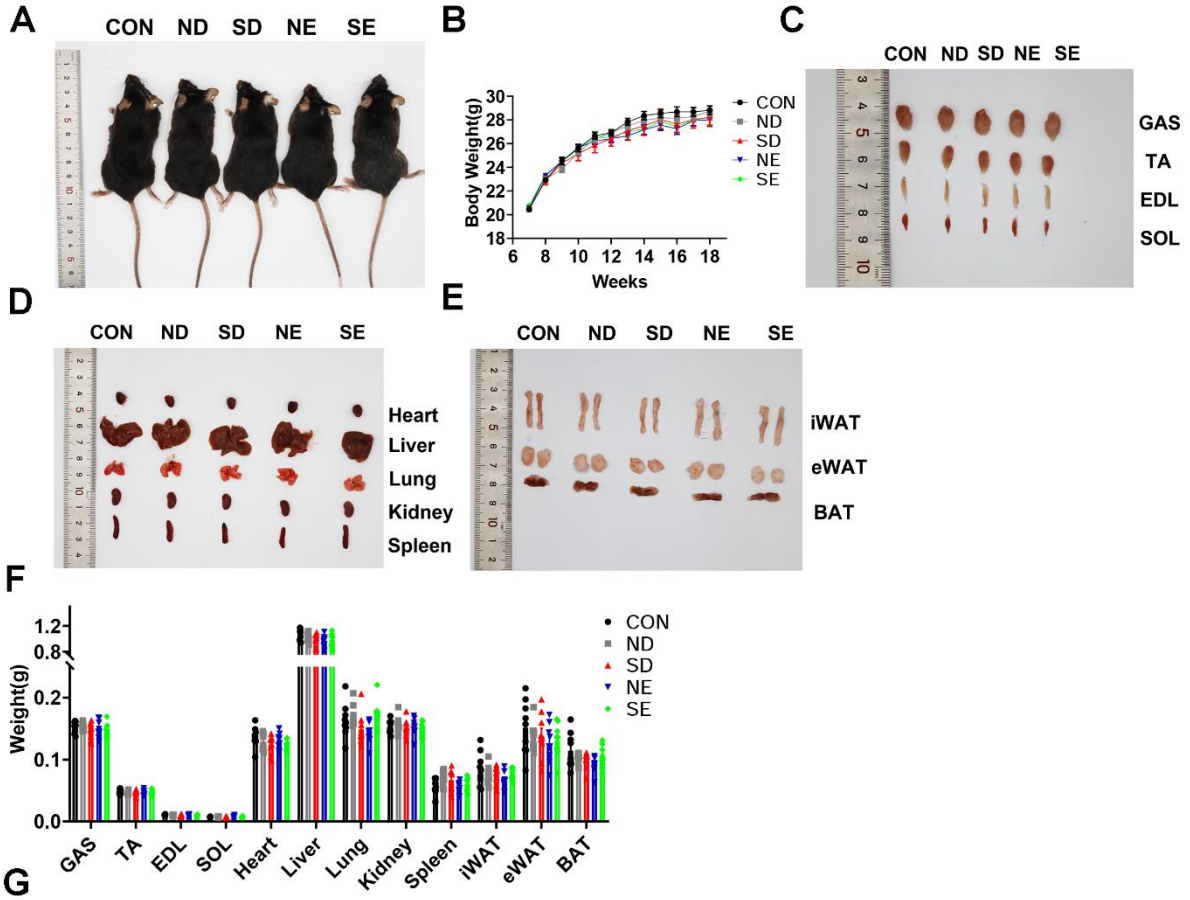

H

Items	CON	ND	SD	NE	SE	P-value
TP, g/L	63.30±4.97	63.73±3.00	59.50±1.62	60.73±1.14	59.68±2.24	0.166
ALB, g/L	36.25±3.45	36.55±2.05	34.25±1.44	34.75±0.79	32.93±1.56	0.133
GLB, g/L	27.05±1.64	27.18±1.26	25.25±2.24	25.98±0.67	26.75±1.16	0.354
ALB/GLB	1.35±0.10	1.38±0.05	1.35±0.17	1.35±0.06	1.25±0.06	0.455
TBIL, μmol/L	2.89±0.87	3.29±0.45	2.78±0.97	3.01±0.66	3.71±1.19	0.582
ALT, U/L	40.00±4.32	38.50±7.33	51.50±37.12	39.75±9.95	39.75±3.30	0.824
AST, U/L	211.75±53.06	169.00±40.93	147.00±46.46	146.50±41.25	132.75±28.78	0.132
AST/ALT	5.24±0.81	4.51±1.24	3.35±1.00	3.79±0.96	3.40±0.99	0.081
GGT, U/L	0.88±0.49	1.25±0.70	1.53±0.10	0.88±0.64	0.55±0.77	0.216
ALP, U/L	61.75±3.77	64.50±7.33	66.00±10.49	63.50±10.08	54.50±8.74	0.377
TBA, μmol/L	6.87±1.24	5.63±0.99	5.49±1.03	4.82±1.68	4.69±2.37	0.33
AMY, U/L	982.25±89.38	1114.00±143.12	1123.75±241.78	977.75±194.29	968.25±133.04	0.507
TG, mmol/L	$1.30±0.20^{a}$	$1.16±0.07^{a}$	$0.91±0.22^{b}$	$0.77±0.08^{b}$	$0.74±0.07^{b}$	<0.001
CHOL, mmol/L	$3.94±0.39^{ab}$	$4.04±0.26^{a}$	$3.16±0.40^{c}$	$3.50±0.35^{bc}$	$3.27±0.19^{c}$	0.005
GLU, mmol/L	6.14±1.29	5.39±1.47	4.85±0.39	7.10±0.61	6.59±1.32	0.072
CRE, μmol/L	43.00±15.10	44.50±24.01	41.25±15.20	38.75±17.52	69.00±16.43	0.166
BUN, mmol/L	11.65±2.01	11.38±1.44	12.33±2.81	12.60±1.47	10.22±0.78	0.42
BUN/CRE	74.25±32.45	72.75±25.67	82.75±33.95	88.25±22.46	39.00±13.54	0.135
tCO2, mmol/L	19.25±1.71	20.00±1.15	21.00±1.41	20.25±2.22	21.75±1.26	0.269
Ca, mmol/L	$2.52±0.09^{a}$	$2.35±0.10^{b}$	$2.27±0.08^{b}$	$2.28±0.10^{b}$	$2.34±0.04^{b}$	0.007
P, mmol/L	$2.98±0.39^{a}$	$2.67±0.27^{ab}$	$2.26±0.01^{bc}$	$2.18±0.42^{c}$	$2.57±0.23^{abc}$	0.012
Ca*P, mg/dl	$93.25±12.15^{a}$	$78.00±10.46^{b}$	$63.75±2.87^{bc}$	$61.75±13.70^{c}$	$74.50±6.03^{bc}$	0.003
Mg, mmol/L	1.60±0.00	1.60±0.00	1.53±0.08	1.59±0.01	1.59±0.02	0.094

Abstract

Eicosapentaenoic acid regulates glucose uptake in skeletal muscle and significantly affects whole-body energy metabolism. However, the underlying molecular mechanism remains unclear. Here we report that eicosapentaenoic acid activates phosphoglycerate mutase 2, which mediates the conversion of 2-phosphoglycerate into 3-phosphoglycerate. This enzyme plays a pivotal role in glycerol degradation, thereby facilitating the proliferation and differentiation of satellite cells in skeletal muscle. Interestingly, phosphoglycerate mutase 2 inhibits mitochondrial metabolism, promoting the formation of fast-type muscle fibers. Treatment with eicosapentaenoic acid and phosphoglycerate mutase 2 knockdown induced opposite transcriptomic changes, most of which were enriched in the PI3K-AKT signaling pathway. Phosphoglycerate mutase 2 activated the PI3K-AKT signaling pathway, which inhibited the phosphorylation of FOXO1, and, in turn, inhibited mitochondrial function and promoted the formation of fast-type muscle fibers. Our results suggest that eicosapentaenoic acid promotes skeletal muscle growth and regulates glucose metabolism by targeting phosphoglycerate mutase 2 and activating the PI3K/AKT signaling pathway.

Graphical Abstract